Measurement of the Pionic and Leptonic Decay Asymmetries of Polarized Σ^- with a PEPR System*

D. BOGERT, P. LUCAS, H. TAFT, AND W. WILLIS
Yale University, New Haven, Connecticut 06520
and
Brookhaven National Laboratory, Upton, New York 11973

AND

D. BERLEY AND P. YAMIN†
Brookhaven National Laboratory, Upton, New York 11973

AND

R. KOFLER, G. MEISSNER, AND S. YAMAMOTO
University of Massachusetts, Amherst, Massachusetts 01002

(Received 9 February 1970)

We have measured the asymmetry parameter α_- for the nonleptonic decay $\Sigma^-\to n+\pi^-$ as well as the asymmetry parameter $\alpha_{\rm lept}$ for the leptonic decays $\Sigma^-\to n+e^-+\bar{\nu}_e$ and $\Sigma^-\to n+\mu^-+\bar{\nu}_\mu$, using polarized Σ^- produced in the reaction $K^-+p\to\Sigma^-+\pi^+$ in the vicinity of the $\Lambda(1520)$ resonance. Measurements were carried out on the Yale Precision Encoding and Pattern Recognition (PEPR) system, and leptonic decays were subjected to gap-length analysis. Using the Σ^- polarization function of Thompson, we find $\alpha_-=-0.067\pm 0.011$ based on 60 000 two-body decays; $\alpha_{\rm lept}=+0.23\pm 0.44$ based on 44 electron decays; $\alpha_{\rm lept}=+0.36\pm 0.39$ based on 44 electron decays and 19 muon decays. Our value of $\alpha_{\rm lept}$ yields a ratio of axial-vector to vector matrix elements given by $g_A/g_V=-0.33_{-0.85}{}^{+0.39}$, using a sign convention in which this ratio is negative for the neutron. While our data favor a negative sign for this ratio (in disagreement with the Cabibbo theory), a positive sign cannot be excluded.

I. INTRODUCTION

In this paper we report a measurement of the asymmetry parameters in the two-body decay channel and in the $\Delta S=1$ leptonic decay channels of polarized Σ^- hyperons. The available channels and their branching ratios are given in Table I. The data were obtained in an exposure of approximately 10^6 pictures in separated beams of 405 to 440 MeV/c K^- mesons at the alternating gradient synchrotron (AGS) using the BNL-Columbia 30-in. liquid-hydrogen bubble chamber. These beam momenta correspond to 375 and 415 MeV/c at the center of the chamber. At these momenta, the Σ^- are produced largely through the formation of the $I=0$, $J^P=\frac{3}{2}^-$ state $\Lambda(1520)$. The D_{03} resonant amplitude then interferes with the predominantly S-wave background to produce large Σ^- polarization.[1,2]

The leptonic decay angular distribution in the Σ^- rest frame takes the form

$$I(q)\sim 1+\alpha\beta\langle\boldsymbol{\sigma}_\Sigma\rangle\cdot\mathbf{q}, \tag{1}$$

where $\mathbf{q}$ is the (unit) momentum vector of the lepton, $\langle\boldsymbol{\sigma}_\Sigma\rangle$ is the Σ^- polarization, β is the lepton velocity, and α is the asymmetry parameter. In the $V-A$ theory, the weak-interaction Hamiltonian takes the form $H=\frac{1}{2}GJ_\lambda j_\lambda$, where j_λ is the lepton current $\psi_e\gamma_\lambda(1+\gamma_5)\psi_{\nu_e}$ and the baryon current J_λ is given by

$$J_\lambda=\psi_p\gamma_\lambda(g_V-g_A\gamma_5)\psi_n+(\text{terms for other hadrons}). \tag{2}$$

Throughout this article, we use the sign convention of Dalitz[3] and of Gershwin *et al.*[4] Assuming time-reversal invariance and neglecting recoil and weak magnetism effects, the asymmetry parameter for leptonic decays is given (approximately) in this theory by[5]

$$\alpha=-2(g_A/g_V)\frac{1+g_A/g_V}{1+3(g_A/g_V)^2}. \tag{3}$$

Thus a measurement of the asymmetry parameter yields information on the g_A/g_V ratio for the relevant decay channel.

In the Cabibbo theory of weak interactions,[6] the baryon currents are assumed to have the form

$$J_\lambda=\cos\theta\,[J_\lambda(0)^V+J_\lambda(0)^A]+\sin\theta\,[J_\lambda(1)^V+J_\lambda(1)^A], \tag{4}$$

where $J_\lambda(0)$ refers to $\Delta S=0$ decays and $J_\lambda(1)$ refers to $\Delta S=1$ decays. In addition, these currents are assumed

* Work supported in part by the U. S. Atomic Energy Commission and the National Science Foundation (Yale Report No. 2726-563), AEC contract AT(30-1)2726.

† Present address: Physics Department, Rutgers University, New Brunswick, N. J.

[1] M. B. Watson, M. Ferro-Luzzi, and R. D. Tripp, Phys. Rev. **131**, 2248 (1963).

[2] J. K. Kim, Phys. Rev. Letters **19**, 1074 (1967).

[3] R. H. Dalitz, in *Weak Interactions and High-Energy Neutrino Physics*, edited by T. D. Lee (Academic, New York, 1966), p. 206.

[4] L. K. Gershwin, M. Alston-Garnjost, R. Bangerter, A. Barbero-Galtieri, F. Solmitz, and R. Tripp, Phys. Rev. Letters **20**, 1270 (1968). See also L. Gershwin, thesis, UCRL Report No. UCRL 19246 (unpublished).

[5] G. Källén, *Elementary Particle Physics* (Addison-Wesley, Reading, Mass. 1964), p. 361.

[6] N. Cabibbo, Phys. Rev. Letters **10**, 531 (1963).

to transform under $SU(3)$ like members of an octet. The conserved-vector-current hypothesis then restricts the vector current to F-type (antisymmetric) couplings, while the axial-vector current may have arbitrary D-type (symmetric) and F-type couplings whose strengths are denoted by d_A and f_A, respectively.

Several authors[7–10] have made fits to the available data finding generally good agreement with the Cabibbo theory. The most recent fit[10] gives

$$\theta=0.234\pm0.006,\ d_A=-0.74\pm0.02,\ f_A=-0.49\pm0.02.$$

A second solution for (d_A,f_A), permitted by the theory, is now eliminated as unlikely on the basis of these fits. Since in the Cabibbo theory the value of g_A/g_V for the channel $\Sigma^-\to nl\nu$ is given by $-d_A+f_A$, this solution predicts $g_A/g_V=+0.25$ and thus the result that $\alpha_{\Sigma^-\to e^-}=-0.526$. The Maryland group[11] has recently obtained a value for $|g_A/g_V|$ of $0.26_{-0.08}^{+0.12}$ for this channel by measuring the e-ν angular correlation. Since the magnitude of g_A/g_V is thus in good agreement with the prediction, a determination of the sign becomes important.

The measurements here reported represent the first application of the Yale PEPR system[12] to an experiment. A similar experiment done with a spiral reader has already been reported by Gershwin *et al.*[4] with a statistical accuracy approximately equal to that reported here. Since the Yale PEPR system is a completely automatic measuring system, the redetermination of the nonleptonic asymmetry parameter also serves as a valuable indication of the limitations and biases of such a device.

II. BEAM AND EXPOSURE

The general purpose of the exposure of 1.3×10^6 pictures at the BNL-Columbia 30-in. chamber, of which the results here reported are only a part, was to study various modes of hyperon decay in the vicinity of the $\Lambda(1520)$. The desire to study, for example, the nonleptonic modes of decay of polarized Σ^+ resulted in about 45% of the exposure being made with a K^- momentum (entering the chamber) of 405 MeV/c, which corresponds to about 375 MeV/c at the center. While the polarization function for Σ^- is not zero in this region, neither is it maximum. The remaining 55% of the exposure was made with the K^- momentum (entering) at 440 MeV/c corresponding to 415 MeV/c at the center, more or less optimum for the production of polarized Σ^-.

TABLE I. Decays of Σ^- and their branching ratios.[a]

Decay	Branching ratio
$n\pi^-$	$\approx100\%$
$ne^-\bar{\nu}_e$	$(1.08\pm0.05)\times10^{-3}$
$n\mu^-\bar{\nu}_\mu$	$(0.48\pm0.06)\times10^{-3}$
$\Lambda e^-\bar{\nu}_e$	$(0.60\pm0.06)\times10^{-4}$
$n\pi^-\gamma$	$<10^{-3}$

[a] Particle Data Group, Rev. Mod. Phys. **41**, 109 (1969).

The K^- were produced at the Brookhaven AGS by rapid beam deflection on a beryllium target at a production angle of 12°. A two-stage electrostatically mass-separated beam was used to transport the K^- at a momentum of 750 MeV/c. Immediately before the chamber, about 90 cm of polyethylene was inserted in the beam to degrade the K^- to the desired momentum.

The 30-in. chamber is an approximate cylinder 72 cm in diameter and 34 cm in depth (z axis). A magnetic field of about 13.4 kG along z, uniform to 13% and known throughout the chamber, was used to distinguish the charge and to measure the momenta of particles passing through the chamber. The exposure was obtained in nine separate runs over a period of approximately one year.

III. SCANNING

The entire exposure was doubled scanned in view 2 for the Σ^- event topology. The scanners were instructed to record every two-prong event with a kink in the negative prong. Strict adherence to this rule, however, would have resulted in the addition of a substantial background of $K^-+p\to K^-+p$ scatters, with the K^- subsequently decaying into a final state with a single charged particle. This contamination was substantially reduced with the following additional rules:

(1) No event with the negative prong produced at an angle larger than 70° to the beam was accepted. This rule eliminated K^-p scatters exclusively, since Σ^- may not be produced, for a K^- beam momentum higher than 300 MeV/c, at an angle greater than 70° in the lab.[13]

(2) No event with the decay occurring more than 8 cm in space from the production vertex was accepted. This rule eliminated K^-p scatters almost exclusively. A Σ^- would have to travel more than $3\frac{1}{2}$ lifetimes even at a high production momentum to reach this length.

(3) It was required that the positive prong at production be at least 3 cm long in two or more views.

[7] W. Willis, H. Courant, H. Filthuth, P. Franzini, A. Minguzzi-Ranzi, A. Segar, R. Engelmann, V. Hepp, E. Kluge, R. Burnstein, T. Day, R. Glasser, A. Herz, B. Kehoe, B. Sechi-Zorn, N. Seeman, and G. Snow, Phys. Rev. Letters **13**, 291 (1964).

[8] N. Brene, L. Veje, M. Roos, and C. Cronström, Phys. Rev. **149**, 1288 (1966).

[9] C. Coulson, Phys. Rev. **152**, 1433 (1966).

[10] H. Filthuth, in Proceedings of the Topical Conference on Weak Interactions, CERN, Geneva, 1969 (unpublished).

[11] A. Colleraine, T. Day, R. Glasser, R. Knop, B. Sechi-Zorn, and G. Snow, Phys. Rev. Letters **23**, 198 (1969).

[12] P. Bastien, T. Watts, R. Yamamoto, M. Alston, A. Rosenfeld, F. Solmitz, and H. Taft, *Methods in Computational Physics* (Academic, New York, 1966), Vol. 5, p. 100. See also I. Pless, L. Rosenson, P. Bastien, B. Wadsworth, T. Watts, R. Yamamoto, M. Alston, A. Rosenfeld, F. Solmitz, and H. Taft, in *Proceeding of the Twelfth International Conference on High-Energy Physics, Dubna, U.S.S.R., 1964* (Moscow, U.S.S.R., 1964), Vol. 2, p. 409; and the status report presented in Proceedings of the International Colloquium on PEPR, University of Nijmegen, 1968, (unpublished).

[13] L. Leipuner, BNL Report No. BNL 945 (T-391), 1965, p. 170 (unpublished).

This eliminated K^-p scatters with short recoil protons since the π^+ must leave the chamber in the Σ^- production configuration. It also eliminated genuine $\Sigma\pi$ where the π^+ was very steep or the π^+ underwent πp scatter. These are both calculable biases at production and presumably unbiased toward the study of Σ^- decay asymmetries.

A fiducial volume was imposed on the scanning; no event with the production vertex lying closer to the edge than 5 cm in space in view 2 (in a radial sense) was accepted. Eventually, a more complicated fiducial volume was imposed inside the PEPR measuring program.

A scanning rule which did directly affect the decay spectrum involved the rejection of any event for which the decay angle was less than 7° in view 2. This was an attempt to impose uniformity on the ability of individual scanners to detect small kinks in a two-prong event. This rule also helped to eliminate genuine two-prong events such as $\Lambda\pi\pi$ events where a scanner might have felt that some unusual fluctuation in ionization near the production vertex was in fact a forward decay.

One additional scanning rule rejected all "collinear" $\Sigma^-\pi^+$ events, unless the Σ^- was produced directly forward. This rule removed Σ^- events produced from stopping K^-. Such Σ^- would be unpolarized and of no use to this experiment.

When an event satisfying the scanning criteria was found, the location of the production vertex was recorded in all three views. This location was determined by using the existing fiducial patterns on the film to form a rough master grid. The fiducial pattern was further subdivided into an 8×8 subgrid, and recorded directly by the scanner onto an IBM "prepunch" card. All three views were recorded since the beam was spread in depth owing to small scatters in the polyethylene degrader. Thus, one could not predict the location of the production vertex in the other two views from only one view. Two views would have been sufficient to determine the location of the production vertex in the third view, but it was found that the third view was valuable as a redundancy check on the scanning, and could be used to correct, by programming, errors in scanner recordings. In addition to the frame number and the grid location of the vertex in three views, the length of the Σ^- in each view was recorded to the nearest cm in space (from 0 to 8 cm). The scanning was performed in conjunction with a scan for the τ^- mode of K^- decay of the beam. This provided a useful check on scanning efficiency for Σ^-.

Approximately 125 000 Σ^- were found as the result of the double scan. The raw scanning data were carried along with the measurements and remeasurements, and into the final library tapes, and final scanning efficiency checks on any particular configuration were possible at the conclusion of the experiment.

IV. MEASUREMENT

A. Yale PEPR System Hardware

PEPR is an acronym for a Precision Encoding and Pattern Recognition device first proposed and developed by Pless and Rosenson.[14] It is in brief, a computer-controlled precision cathode-ray tube (CRT). A block diagram of the Yale PEPR system is shown in Fig. 1. Deflection and focusing of the electrostatically accelerated electron beam is accomplished entirely by iron-cored yokes whose windings are fed by drivers controlled by a number of digital-to-analog converters (DAC's). The optically flat face of this 5-in. tube is focused on the film to be scanned, and the transmitted light is collected on the face of an RCA 8575 photomultiplier tube. Present techniques in the construction of phosphors, focusing yokes, and electron guns permit the generation of a spot with a half-intensity width of approximately 25 μ. A distinctive feature of PEPR, however, is the introduction of an additional yoke wound as a magnetic diquadrupole. If one introduces a current proportional to $\cos\theta$ (the M function) in one of the windings of the diquadrupole, and a current proportional to $\sin\theta$ (the N function) in the other, then a line whose physical angle is $\theta+\delta$ (where δ is a constant angle depending on the orientation of the diquadrupole) will be generated in place of a spot on the face of the CRT. The length of this line is proportional to the total current in the diquadrupole, up to saturation. With the yokes as wound for the Yale PEPR, a 25-μ spot can be defocused into a line nearly 2 mm long, while maintaining its 25-μ width. Since the projection lens (6-in. focal length, $f4$) demagnifies by 1.5:1, this line appears on the film as approximately 1.33 mm long and 17 μ wide.

During operation, this line is swept along either the x or the y axis (whichever is more perpendicular to the line direction) at a writing speed of 200 μ/μsec. Since the film is normally developed from a bright field exposure (appearing on the film as clear tracks on a dark background), the photomultiplier anode produces a negative pulse whenever the image of the line traverses a track on the film. It is clear that the pulse height and width depend critically on the relative orientation of the track and the line image. Figure 2 shows the theoretical pulse shape as a function of this orientation, and Fig. 3 shows an actual pulse from a track parallel to the line. The "pedestal" results from the transmission of light through the exposed film whenever the CRT is unblanked.

The angle dependence of pulse height and width enables one to measure the direction of a track by means of a pulse sampling circuit. The particular circuit employed was developed at MIT,[12] and is known as a track element detector (TED). This TED circuit

[14] I. A. Pless and L. Rosenson, MIT Laboratory for Nuclear Science report, 1962 (unpublished).

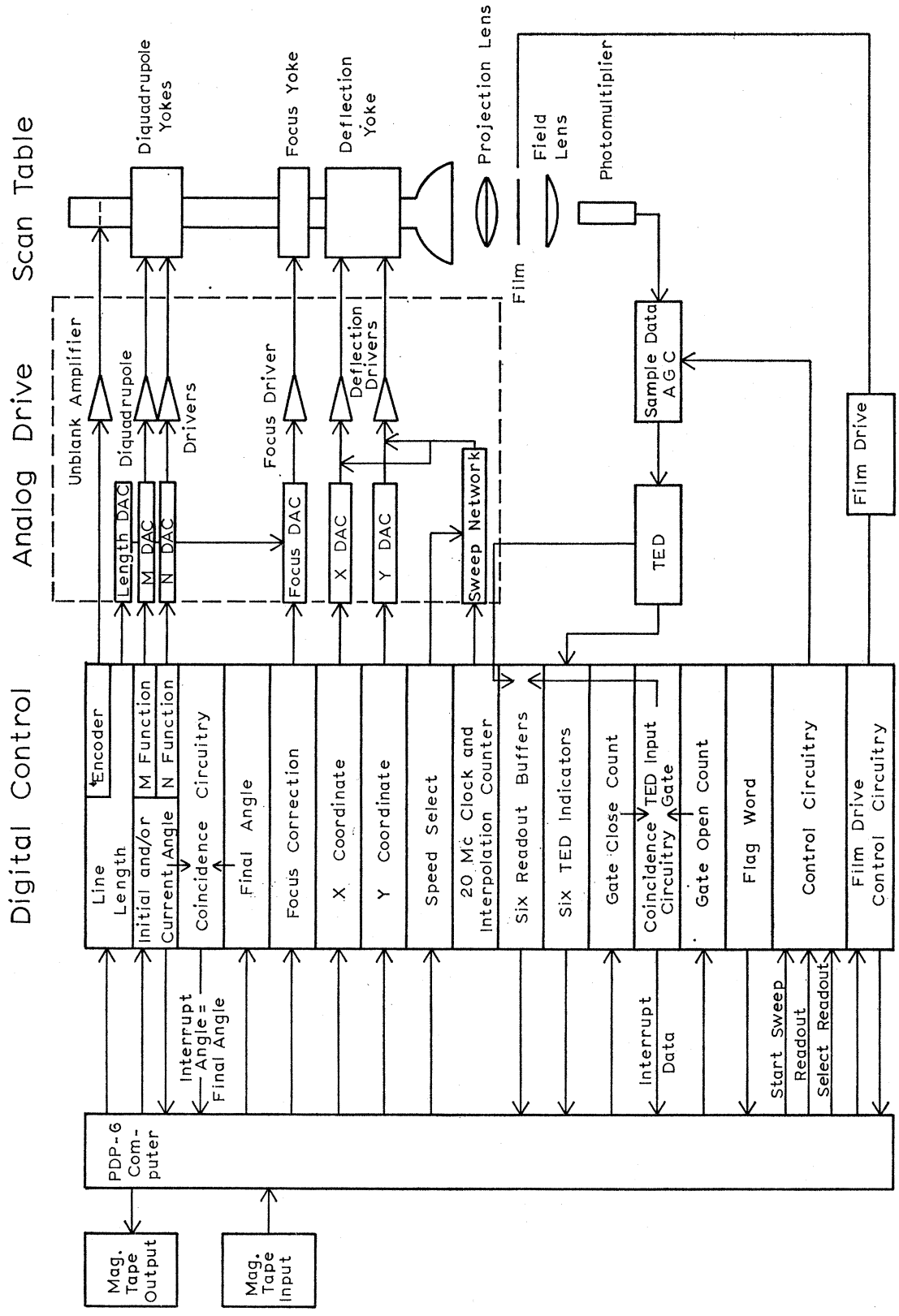

FIG. 1. Block diagram of the Yale PEPR system.

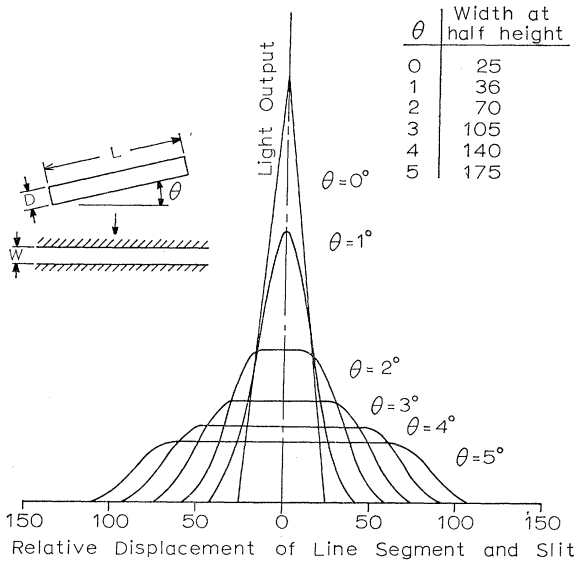

FIG. 2. Sketch of the theoretical light output from a slit crossed by a line segment having a uniform intensity distribution. In this case the line width D is assumed to be equal to the slit width W, and the line length L is assumed to be 80 times the width D. θ is the relative angle between the slit and line orientations.

is essentially a series of delay line buffers of different lengths which sample the pulse at different points. Height and width criteria are then imposed, which in principle limit the acceptance to tracks within about $\pm 4°$ of the line direction. Large variations in background opacity (more than 8:1) required the use of an automatic gain control circuit (AGC) before successful operation over entire pictures was obtained.

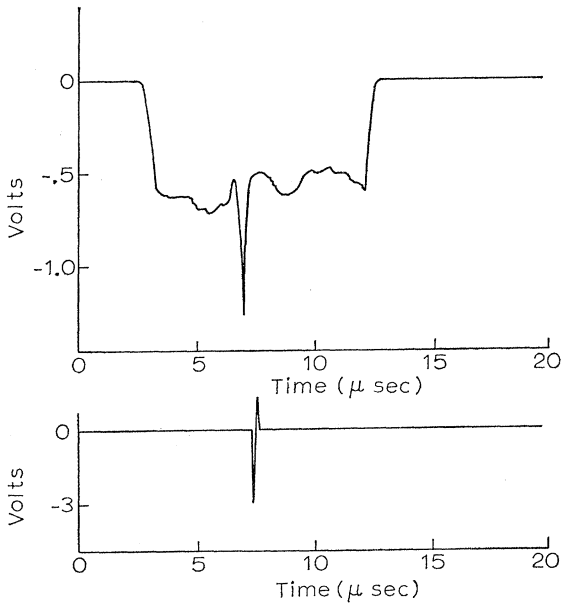

FIG. 3. An actual track pulse is illustrated in the upper trace, which is a sketch of the phototube output. The sharp pulse is a track pulse. The flat background (or pedestal level) is due to light transmitted through the only partially opaque film. The lower trace represents a T.E.D. output pulse generated after the track pulse satisfied height and width criteria. This pulse will stop a scaler which was started when the sweep was started.

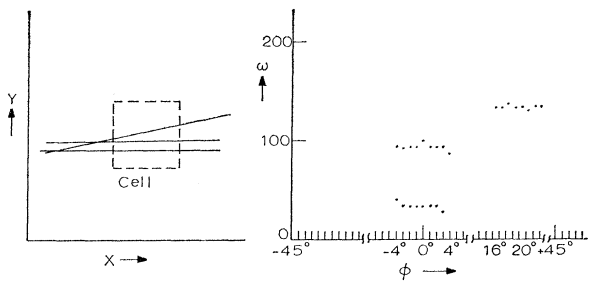

FIG. 4. These two sketches illustrate the principles of "Element Recognition." The left-hand sketch represents three idealized tracks passing through a 1.3×1.3-mm square cell on the film. The right-hand sketch represents the idealized T.E.D. hits corresponding to the track pattern sketched to the left. The right-hand sketch is known as a (ϕ,ω) plot in which clock counts ω are plotted against the current angle ϕ. The "element recognition" program examines the (ϕ,ω) array and groups the T.E.D. hits into track elements of an average ϕ and ω.

The actual sweep is initiated by a digital control unit which simultaneously starts six 20-Mc scalers. These scalers are turned off (in sequence) whenever an acceptable pulse is indicated by the TED circuits at a given angle. The track position may then be determined by combining the (x,y) position of the sweep center with the appropriate scaler reading. With this sweep speed, the least count of this system corresponds to $6\frac{2}{3}\,\mu$ on the film. Instabilities and nonreproducibilities in the system are less than the least count.

In addition to sweep start and restart logic, the digital control unit contains wired-in angle functions, as well as flags, gates, and registers which may be loaded and unloaded by the Digital Equipment Corporation PDP-6 computer used to control the system. Once initialized, the digital control will perform sweeps at successive angles until either data is obtained, or a prespecified angle is reached. At this point any data must be read out of the digital control unit by the computer, and the sweep cycle restarted. Since the x and y registers are 12-binary bits, one may center the sweep at any point on a 4096×4096 raster. All pincushion and other distortions in this system are removed through software rather than hardware corrections.

Calibration of the system involves the measurement of a calibrated grid. First, one must determine the relationship of the sweep-scaler counts to the x, y counts. Second, a set of 35 measurements of known points is performed over the CRT face at line angles of 0° and 90°, and a 21-term polynomial is fitted to these measurements. Third, a series of measurements at different angles over the CRT face is used to construct a function which is an angle-dependent position correction, vanishing at 0° and 90°. It is found empirically that these three correction functions are sufficient to map a set of 60 points, measured at 0°, 45°, 90° and 135°,

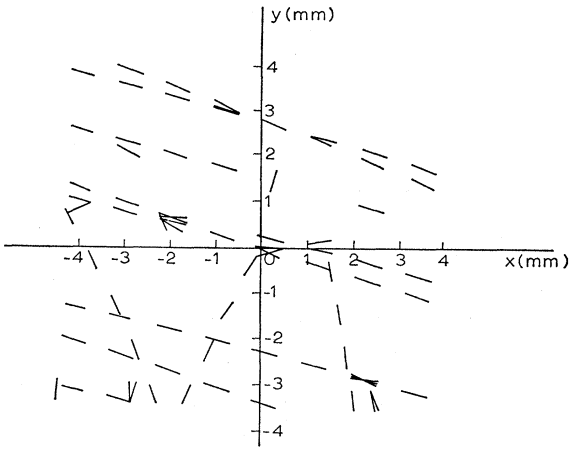

FIG. 5. Elements found in an 8×8 raster scan centered on a Σ^- event. All elements that have been found within an 8×8-mm region centered on the scan zone are displayed. The step between the raster lines is 1 mm.

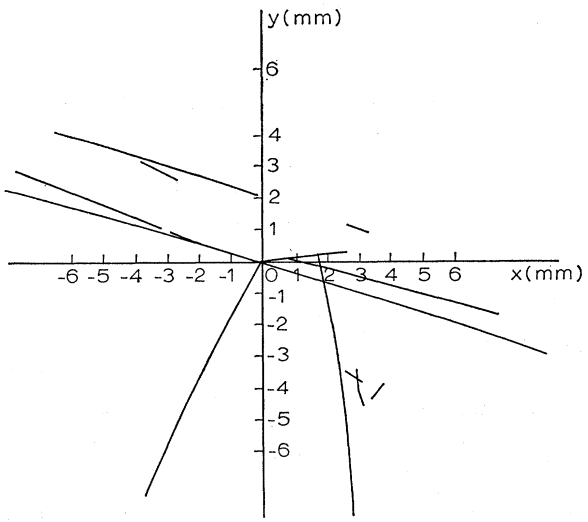

FIG. 6. Tracks which have been generated after elements from the raster scan of Fig. 5 have been linked by a track-following routine. Through background tracks have been removed.

ranging over the entire CRT face, to an absolute grid with mean residuals smaller than 5 μ. The calibration procedure takes about 10 min and is normally repeated every few hours.

B. Yale PEPR System Software

PEPR software has been discussed in several publications[12] and will only be summarized here, except for the program used to identify the prescanned Σ^- production configuration. Since data are obtained whenever the line is within $\pm 4°$ of a track, the lowest level programs simply extract the clock count w at sequential angles, and group the data from separate tracks into "track elements" as indicated in Fig. 4. Working with these "track elements," the main sections of the program perform in sequence:

(1) Three fiducial measurements, after the film has been positioned under computer control. These measurements contain sufficient redundancy to check that the proper fiducials are indeed found and enable the program to locate the zone in which the scanner recorded the event.

(2) A raster scan, in which all track elements in the vicinity of the scan zone are obtained. Typical results of this procedure are shown in Fig. 5.

(3) An element linking procedure, using a track following routine with considerable predictive and logical power, which works from the edge of the raster scan into the center, eliminating elements as it links them into tracks.

(4) A series of routines which eliminate duplicate tracks, break tracks with small kinks, and eliminate tracks which cannot be associated with the event. Typical results of Secs. (3) and (4) are shown in Fig. 6.

(5) An event type program, which selects tracks satisfying the scan topology and follows these tracks to the edge of the picture, storing up to ten precision measurements appropriately spaced along each track in unconfused regions.

For the Σ^- production event considered here, all combinations of beamlike and positive tracks are examined in the order of most likely to least likely event topology. Since the beam energy is low, the Σ^- production is almost always a two-body interaction and visible momentum is conserved in any plane, including (because of optical effects, only approximately) the film plane. Thus, two circles fitted through the K^- and π^+ tracks in the film plane may be used to determine (approximately) the direction of the Σ^-. If the Σ^- is long enough (which information is also provided on the prescan input) a search at the suspected location of the

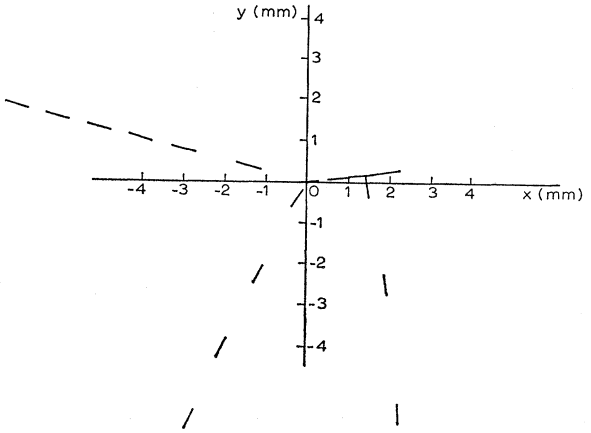

FIG. 7. Σ^- as deciphered in the region of the production and decay vertices. The tracks will now be followed to the edge of the picture or to their respective end points.

FIG. 8. Points selected for final measurement on the tracks of the Σ^- event after they had been followed to the edge of the picture or to their end points.

Σ^- is initiated. If found, the Σ^- is followed to its end and a second small raster scan is performed at this point. This is followed by the routines in Secs. (3) and (4) mentioned above. A (logical) search is then made for a possible decay candidate, and if a satisfactory candidate is found, it is followed and measured. Decay track candidates not within $\pm 10°$ of the beam direction are preferred in order to eliminate noise arising from beam track segments not properly handled. In the case of a Σ^- too short to be detected by PEPR, a decay track in conjunction with a $K^-\pi^+$ vertex in the very near vicinity is sought. The results of track identification and final measurement are shown in Figs. 7 and 8.

V. GEOMETRY AND KINEMATICS

A. TVGP and Modifications

All events measured by PEPR are reconstructed using the three-view geometry program (TVGP)[15] in a version coded at BNL for use on the CDC-6600 computer. As originally coded TVGP seeks to reconstruct the trajectory of a track in space as a spiral by projecting the track as viewed in each of the three pairs of cameras back through the front glass onto the film. The program then seeks to minimize the deviations of the measured points in all views in the film plane. If an acceptable minimum corresponding to an orbit inside the chamber cannot be found, the track is failed. During this procedure the program assumes that all measured points in each view are relevant to the track in question. Unfortunately, this assumption is not always valid for PEPR output. For instance, it is not uncommon for PEPR to measure an unrelated track segment in one view while measuring the correct track in the other two views. In order to save such a situation whenever possible, a routine has been inserted into TVGP at the point where a preliminary reconstruction based on three pairs of views has been performed. This routine utilizes the fact that a track which is correctly matched in a view pair will exhibit a linear dependence of the z coordinate on arc length. Whenever such a dependence exists in only one of the three pairs, the view common to the two nonlinear pairs is discarded. Since in most cases two views are sufficient to reconstruct a track, this procedure reduces the number of TVGP track failures substantially. A further but less stringent test is made to ensure that the reconstructed orbits pass sufficiently close to the vertices as measured by PEPR.

The measurement quality of tracks reconstructed by

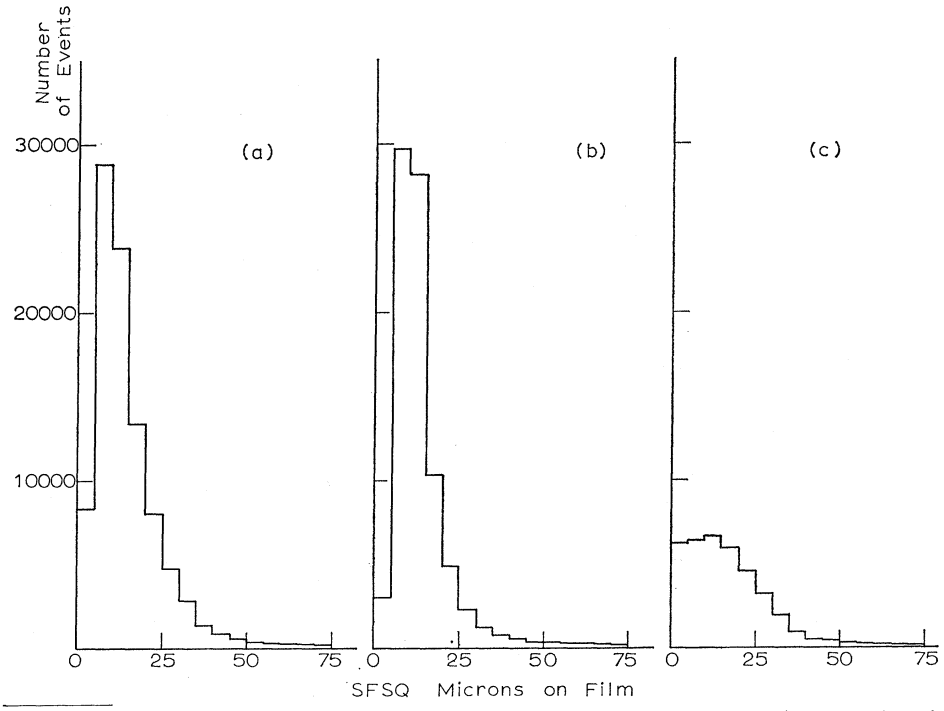

FIG. 9. SFSQ distributions on the K^- for (a) the final sample, (b) the PEPR sample, and (c) the hand-measured sample.

[15] F. Solmitz, A. Johnson, and T. Day, Alvarez Group Programming Note P-117, University of California at Berkeley report, 1965 (unpublished).

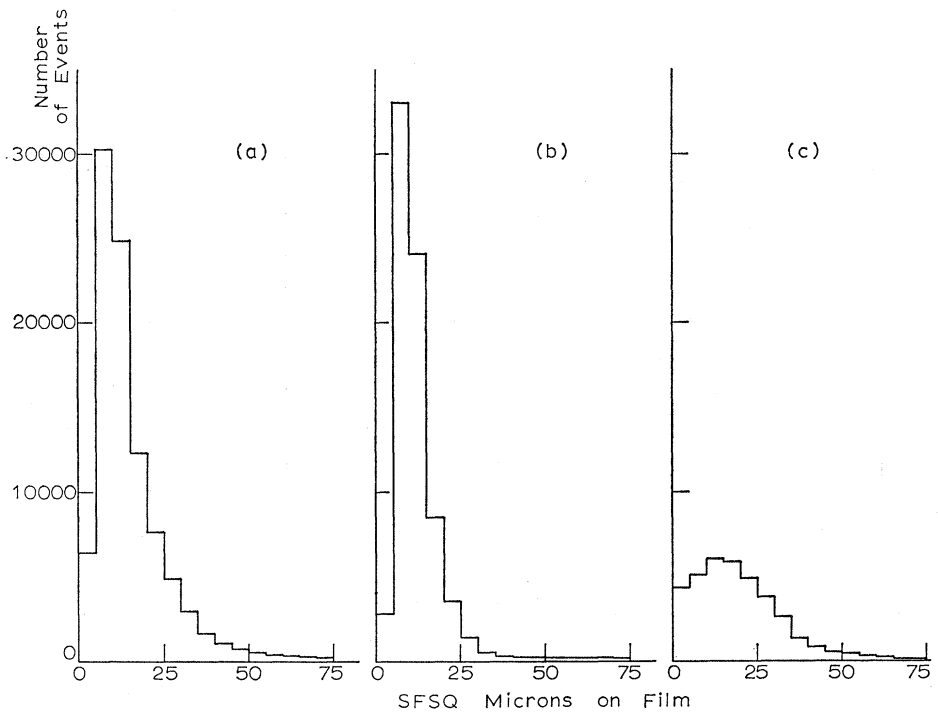

FIG. 10. SFSQ distributions on the π^+ for (a) the final sample, (b) the PEPR sample, and (c) the hand-measured sample.

TVGP may be judged by several criteria. A figure of merit, known as SFSQ, is calculated for each reconstructed track. Essentially, this is the mean (residuals^2/point) in the film plane and for a well-measured track of high momentum will be of the order of the least count of the measuring machine. However, at the low momenta involved in this experiment Coulomb scattering is dominant, and considerably higher residuals are to be expected. Figures 9–11 illustrate SFSQ's for the K^-, π^+ and decay tracks as measured by PEPR. These distributions peak at about 10 μ or less, corresponding to an SFSQ a little larger than the $6\frac{2}{3}$-μ PEPR least count.

Another criterion for judging the quality of PEPR measurements is the measured laboratory beam momentum propagated back to the chamber entrance

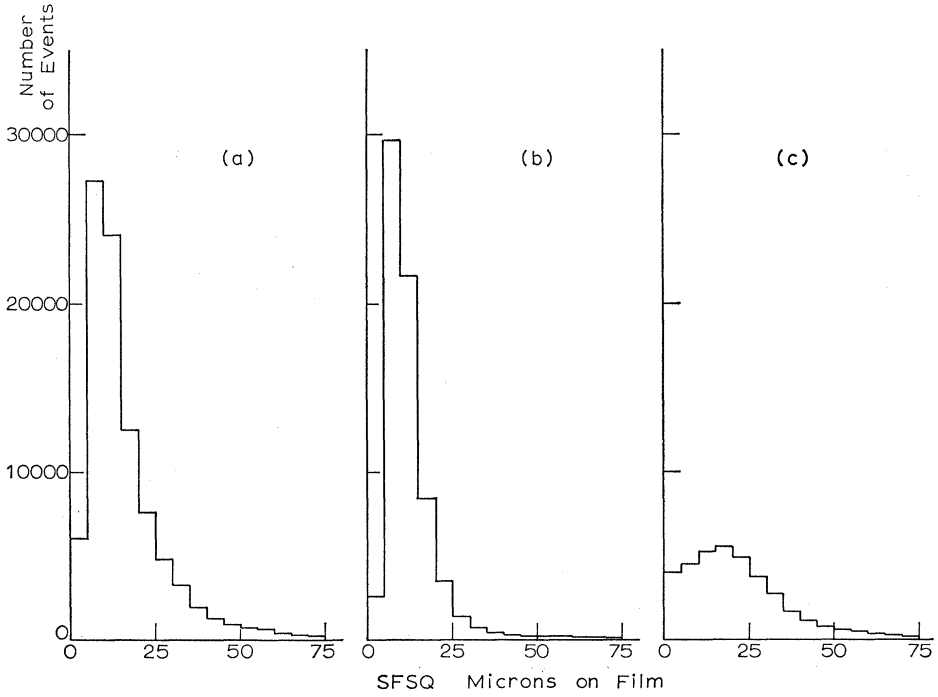

FIG. 11. SFSQ distributions on the decay track for (a) the final sample, (b) the PEPR sample, and (c) the hand-measured sample.

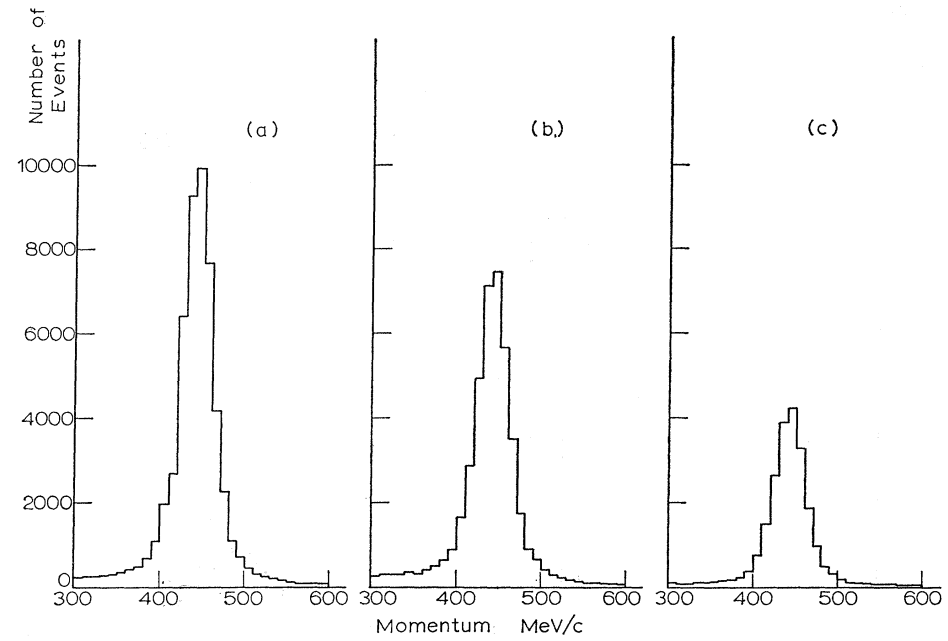

FIG. 12. Beam momentum distributions at the chamber window for K^- entering the chamber at 440 MeV/c for (a) the final sample, (b) the PEPR sample, and (c) the hand-measured sample.

window. Figures 12–15 show such distributions obtained from film taken with degrader thickness adjusted for 440 and 405 MeV/c entering. For comparison, the beam distribution measured on a hand-measuring system is included in each case. The width of the distributions (reflecting the initial momentum spread as well as scattering in the degrader) is somewhat narrower for PEPR measurements than for the hand measurements.

B. Yale Kinematics Program (YACK)

This program uses standard kinematic fitting procedures with an event-type control program and has been described previously.[16] One important addition was made for this experiment, namely, a three-dimensional vertex finding routine. The Yale PEPR system was operated exclusively with a flying line of length 1.33 mm and therefore the measured point closest to

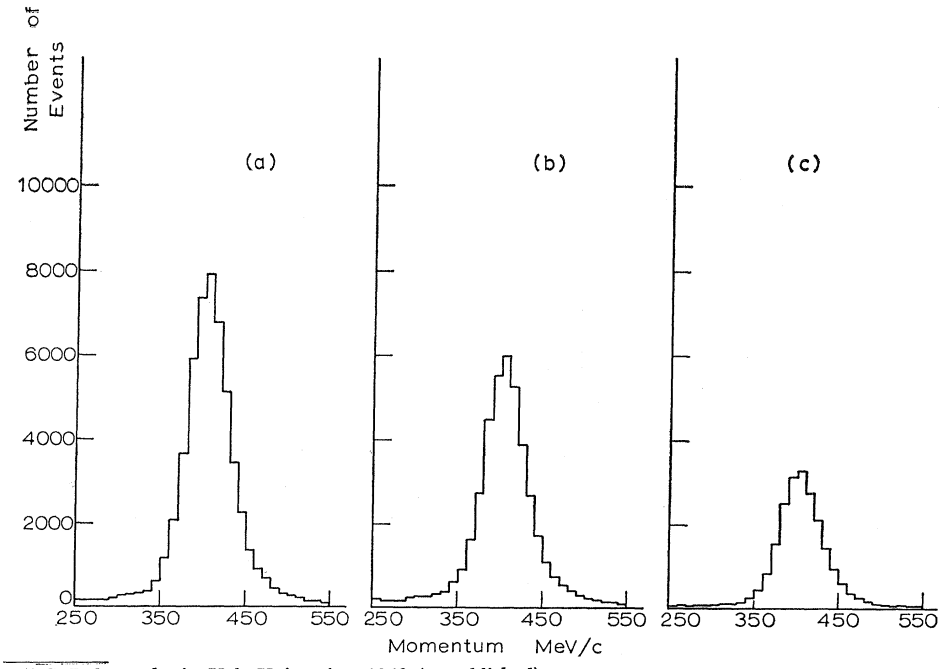

FIG. 13. Beam momentum distributions at production for K^- entering the chamber at 440 MeV/c for (a) the final sample, (b) the PEPR sample, and (c) the hand-measured sample.

[16] C. Baltay, thesis, Yale University, 1963 (unpublished).

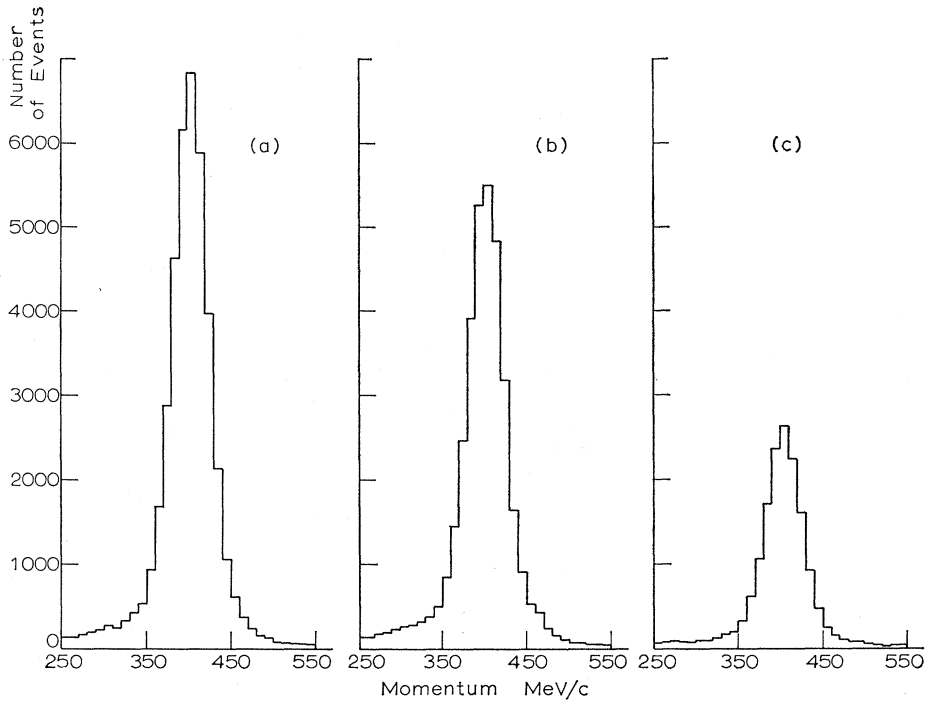

FIG. 14. Beam momentum distributions at the chamber window for K^- entering the chamber at 405 MeV/c for (a) the final sample, (b) the PEPR sample, and (c) the hand-measured sample.

the vertex on a given track was typically 1 mm on the film (about 1 cm in space) out from the vertex. In order to apply the constraints of energy and momentum balance in the fitting procedure, it was necessary to reconstruct a three-dimensional vertex point and to propagate all track variables to the vertex. A routine was therefore employed which found that point in space for which the sum of the squares of the perpendicular distances to the appropriate set of helices (or straight lines if only two points were measured on a track) was a minimum. This routine utilized an iterative procedure which converges in a very large percentage of cases.

The fits tried by the event-type routine used in this

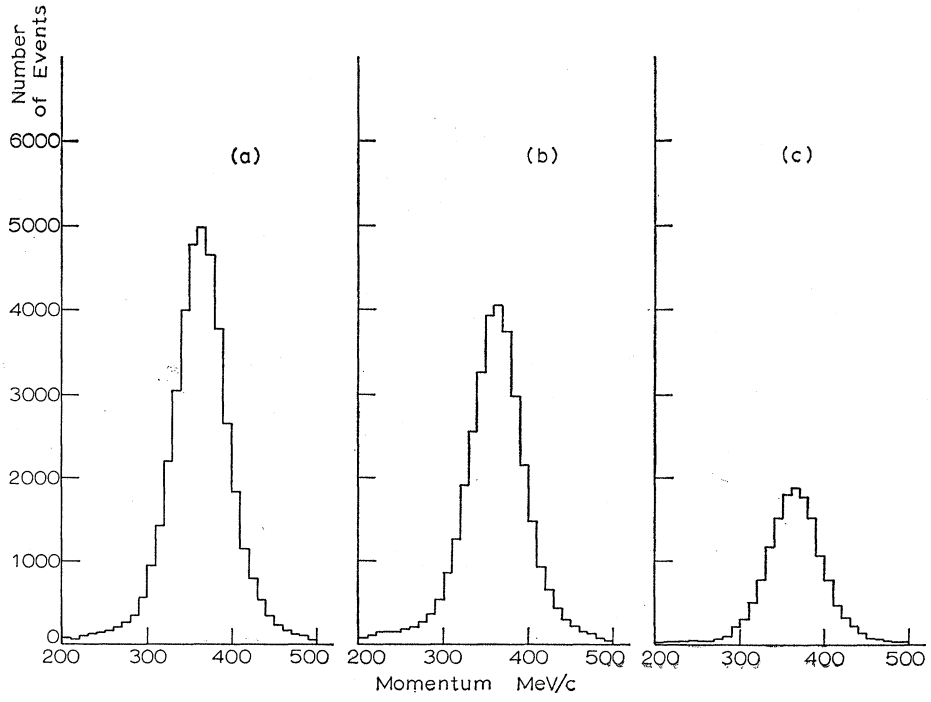

FIG. 15. Beam momentum distributions at production for K^- entering the chamber at 405 MeV/c for (a) the final sample, (b) the PEPR sample, and (c) the hand-measured sample.

TABLE II. Fit descriptions.

Fit number	Event	Constraints	Unmeasured quantities
1	$K^-+p \to \Sigma^-+\pi^+$	3C	Σ^- momentum
2	$K^-+p \to \Sigma^-+\pi^+$	2C	Σ^- momentum, K^- momentum
3	$K^-+p \to \Sigma^-+\pi^+$	2C	Σ^- momentum, π^+ momentum
4	$K^-+p \to \Sigma^-+\pi^+$	1C	Σ^- all
5, 15	$K^-+p \to \Sigma^-+\pi^+$	0C	Σ^- all, K^- momentum (two solutions)
6, 16	$K^-+p \to \Sigma^-+\pi^+$	0C	Σ^- all, π^+ momentum (two solutions)
7, 17	$K^-+p \to \Sigma^-+\pi^+$	0C	K^- all, Σ^- momentum (two solutions)
8, 18	$K^-+p \to \Sigma^-+\pi^+$	0C	π^+ all, Σ^- momentum (two solutions)
51	$K^-+p \to K^-+p$	3C	scattered K^- momentum
52	$K^-+p \to K^-+p$	2C	scattered K^- momentum incident K^- momentum
53	$K^-+p \to K^-+p$	2C	scattered K^- momentum p momentum
54	$K^-+p \to K^-+p$	1C	scattered K^- all
Also, twelve fits numbered 21–28, and 35–38, all of which are			
Decay	$\Sigma^- \to n+\pi^-$	1C	n all

experiment are listed in Table II, with the constraint classes and unmeasured variables indicated. It was always assumed that since the Σ^- track was less than 8 mm long (on the film), no useful measurement of its momentum was possible. The event type was constructed to extract the maximum amount of information from PEPR measurements, which might be partially incorrect. A fit was accepted if the value of the χ^2 was less than five times the number of constraints. Based on previous experience this criteron is a conservative one in that only a small background of "fake" events (other than kinematic ambiguities) will be accepted while marginal events will be flagged for remeasurement. A fit to the decay process $\Sigma^- \to n+\pi^-$ was always attempted after every nonreject production fit, whether accepted or not. A fit to the process $K^-+p \to K^-+p$ was also attempted at every stage of constraint reduction, except for 0C cases, until the process terminated.

If a 3C $\Sigma^-\pi^+$ production fit was accepted together with an acceptable decay fit, processing was stopped. Otherwise the fits listed in Table II were tried in succession until acceptable $\Sigma^-\pi^+$ production and decay fits were obtained. If, after all four constrained fits and the eight 0C solutions were tried, no Σ^- production followed by $n\pi^-$ decay was accepted, the four K^-p scattering fits were examined and if any were acceptable this event was flagged as a possible K^-p candidate. The K^-p acceptance cirteria were later tightened as described below.

It should be noted that if no Σ^- was measured at all, as was the case for any Σ^- recorded during scanning as less than 0.8 mm in length on the film, the process of constraint elimination in YACK had to begin with the 1C Σ^- production fit. If the beam track or π^+ failed, the process began with the 0C solutions in the case of measured Σ^-, and the event was rejected if the Σ^- was unmeasured. This constraint reduction event type, like the TVGP modifications discussed above, was helpful in rescuing blunders committed by PEPR and consequently in reducing the number of remeasurements.

The χ^2 distributions and missing-mass distributions obtained by YACK are shown in Figs. 16–23. Crucial for the selection of leptonic decay events is the distribution of the measured momentum of the decay track transformed to the center of mass of the fitted (from production) Σ^-. Since the normal Σ^- decay mode is two body, this yields a unique π^- momentum of 191.7

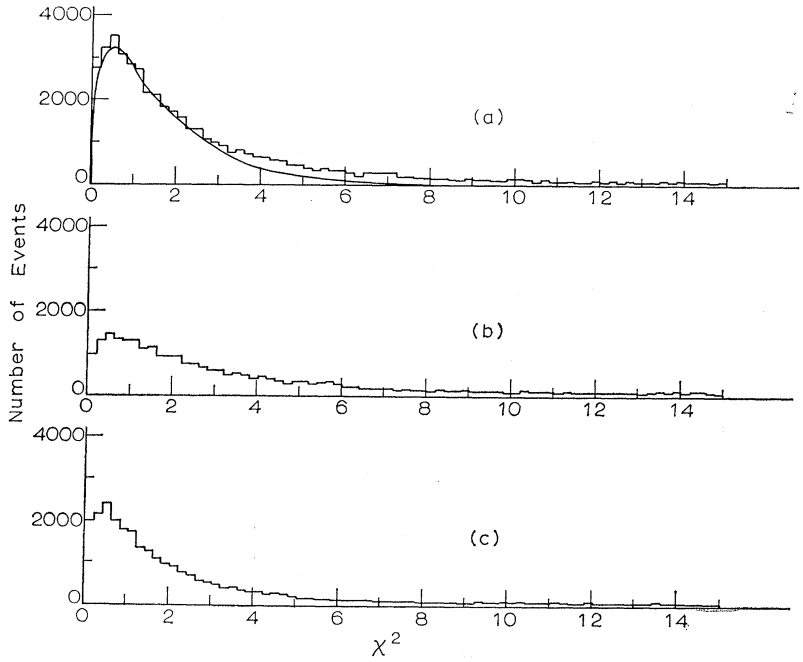

FIG. 16. 3C χ^2 distributions for the $K^-+p \to \Sigma^-+\pi^+$ fit at production for (a) the final sample, (b) the PEPR sample, and (c) the hand-measured sample. In Figs. 16(a)–22(a), a solid line representing a scaled χ^2 distribution of the appropriate constraint class has been fitted to the data. The scale factor used was 0.575. This scaling was necessitated by a misestimation of the measuring accuracy of PEPR in the geometric reconstruction programs. This is a result of the fact that the PEPR measuring error was uniformly somewhat less than originally estimated.

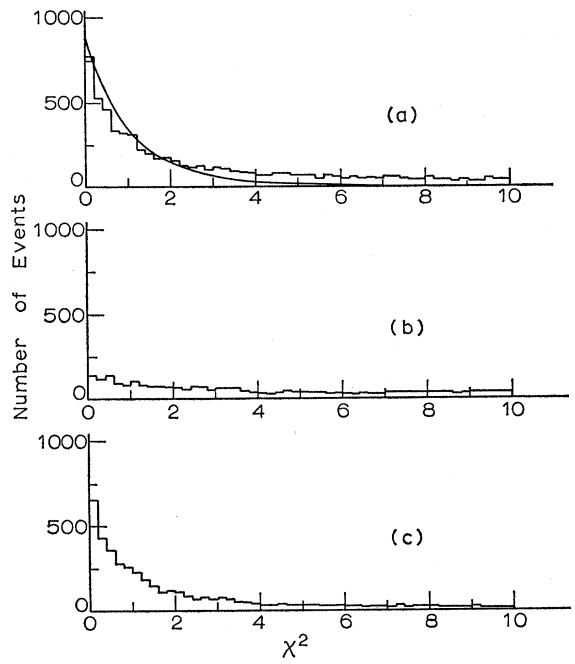

FIG. 17. 2C χ^2 distributions for the $K^-+p \to \Sigma^-+\pi^+$ fit at production for (a) the final sample, (b) the PEPR sample, and (c) the hand-measured sample.

MeV/c.[17] Figure 24 shows this distribution for events making satisfactory decay fits. The two-body decay peak has a full width at half-maximum of about 15 MeV/c. In order to investigate the leptonic decay region this distribution is shown expanded by a factor of 50 in Fig. 25. On the basis of the shape of the low-momentum tail, events with decay momenta (in the fitted Σ^- c.m. system) less than 165 MeV/c were considered candidates for leptonic decays as discussed in Sec. VIII. This cut was eventually lowered to 160 MeV/c.

VI. REMEASUREMENTS

The choice of remeasurement criteria was strongly influenced by the over-all purpose of the experiment, which was, of course, to identify the leptonic decays. The normal "two-body" pionic decay of the Σ^- has a unique center-of-mass momentum of about 192 MeV/c.[17] The leptonic decays are all three-body decays, as is the radiative decay $\Sigma^- \to n\pi\gamma$. The three-body phase-space curves are presented in Fig. 26. The general shape of these curves is suggestive of an approach to separate leptonic decays from the total sample. A momentum cut in the Σ^- center-of-mass system at 165 MeV/c, for example, will remove only 14.3% of the electron spectrum. Even correcting for the misinterpretation of the electron mass as a π (this correction to phase space being accomplished by a Monte Carlo calculation), the fraction of events lost above a cut of 165 MeV/c rises to only 19%, with 81% of the electron decays still possessing a center-of-mass momentum for the decay, interpreted as a π^-, below

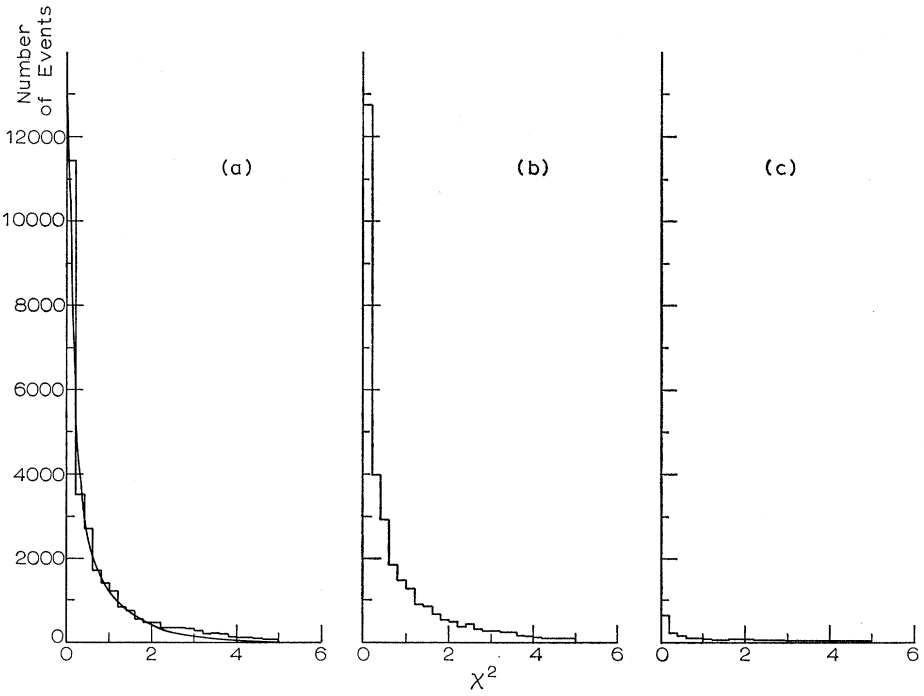

FIG. 18. 1C χ^2 distributions for the $K^-+p \to \Sigma^-+\pi^+$ fit at production for (a) the final sample, (b) the PEPR sample, and (c) the hand-measured sample.

[17] The slight discrepancy with the value found in N. Barash-Schmidt, A. Barbaro-Galtieri, L. Price, A. Rosenfeld, P. Söding, C. Nohl, M. Roos, and G. Conforto [Rev. Mod. Phys. **41**, 109 (1969)] is due to our use of the older value of 1195.96 MeV for the Σ^- mass.

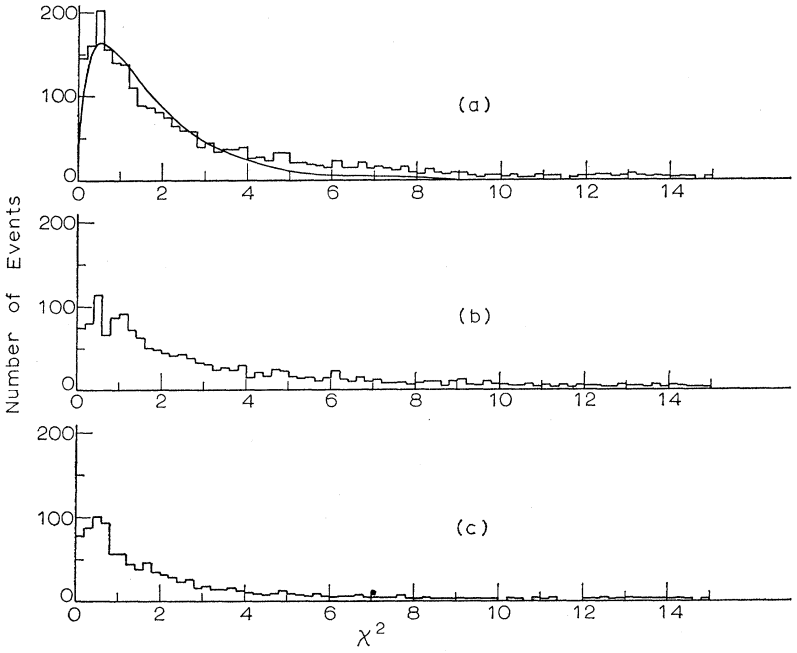

FIG. 19. 3C χ^2 distributions for the $K^- + p \rightarrow K^- + p$ scatter fit for (a) the final sample, (b) the PEPR sample, and (c) the hand-measured sample.

165 MeV/c. A number of authors[18,19] have computed the radiative decay spectrum under the assumption of s-wave or p-wave decay amplitudes. Using the result of Berley *et al.*[20] that the amplitude is predominantly s wave, we have computed the spectrum from Table VIII of Ref. 19, and this is shown in Fig. 26. Above 165 MeV/c the number of radiative decays so dominate the leptonic spectrum that the *a priori* probability of radiative decay would overwhelm any indication of leptonic decays based on gap-length distributions.

The above considerations led to the selection of a set of first remeasurement criteria. A criterion to eliminate K^-p events was also necessary, and it was decided that the definition of a "much better" K^-p fit would be that either it must make a K^-p fit with a higher number of constraints than the Σ^- fit, or it must make a K^-p fit with a χ^2 at least 3.0 better than the Σ^- production fit with the same constraint number. The criteria used selected the following classes of events for remeasurement: (1) any event which failed at least two views on PEPR; (2) any event for which track 4, the decay track, failed and which did not make a "much better" K^-p fit than Σ^- fit at production; (3) any event for which the measured momentum of track 4 translated into the Σ^- rest frame was less than 165 MeV/c and did not make a "much better" K^-p; (4) any event for which the measured momentum of track 4 translated into the Σ^- rest frame was greater than 225 MeV/c and did not make a "much better" K^-p; (5) any event which did not make a constrained production fit unless it made a plausible 0C solution with a good 1C decay fit.

The selection program generated a remeasurement list of all events to be remeasured. About 34% of the entire PEPR sample was remeasured. About one-half of the remeasurements were generated by insufficient

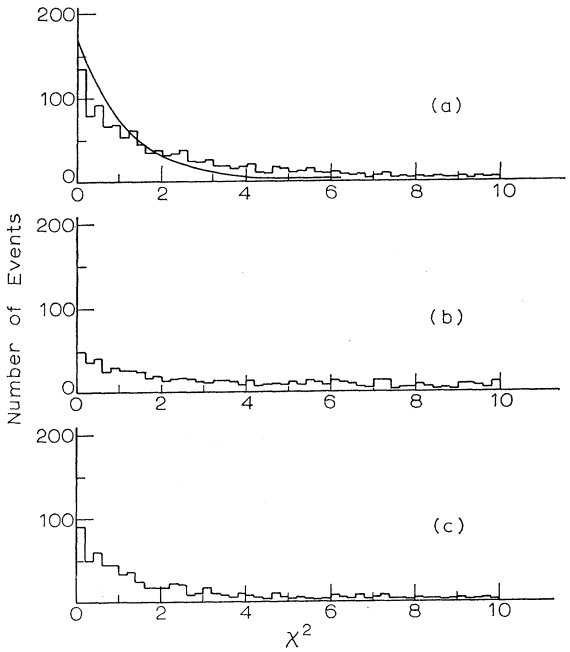

FIG. 20. 2C χ^2 distributions for the $K^- + p \rightarrow K^- + p$ scatter fit for (a) the final sample, (b) the PEPR sample, and (c) the hand-measured sample.

[18] S. Barshay, U. Nauenberg, and J. Schultz, Phys. Rev. Letters **12**, 76 (1964).
[19] M. C. Li, Phys. Rev. **141**, 1328 (1966).
[20] D. Berley, S. Hertzbach, R. Kofler, G. Meisner, J. Shafer, S. Yamamoto, W. Heintzelman, M. Schiff, J. Thompson, and W. Willis, Phys. Rev. Letters **19**, 979 (1967).

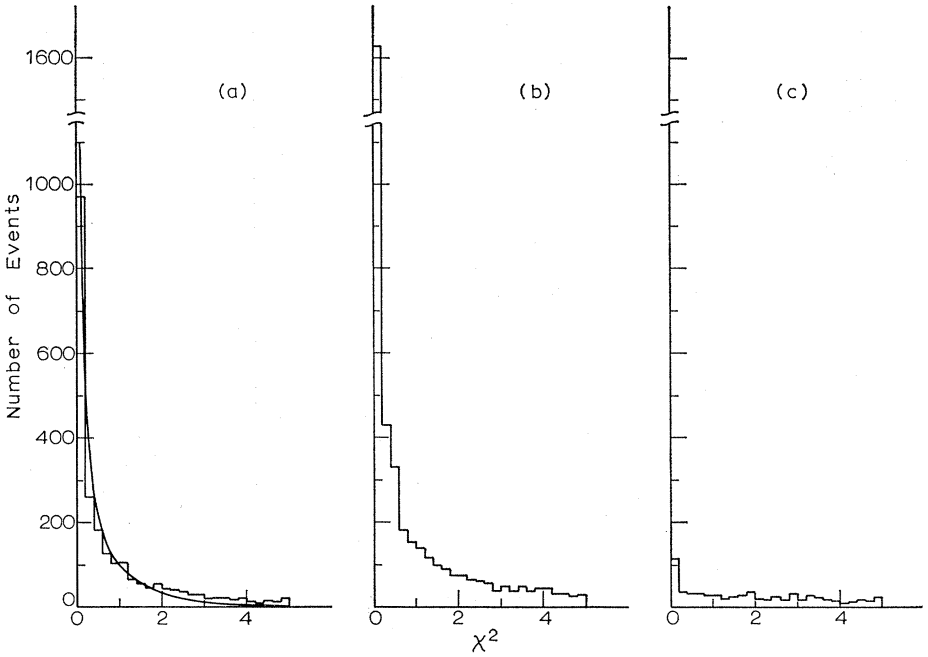

FIG. 21. 1C χ^2 distributions for the $K^-+p \rightarrow K^-+p$ scatter fit for (a) the final sample, (b) the PEPR sample, and (c) the hand-measured sample.

views measured by PEPR; the other half was predominantly generated by a missing decay track. The number of events with four reconstructed tracks and no fit was small.

Thus, about 42 000 events were selected for remeasurement after the pass through PEPR. The entire remeasurement sample was measured in a "three-point, three-view" format. About 22 000 events were measured at BNL on "Mangiaspago" machines. The remaining 20 000 events were measured at Yale on "wire measuring machines," so named because their active component is a piece of magnetostrictive wire.

The output tapes from BNL and the Yale wire measuring data were standardized in format, and frame-ordered by roll. A comparison was made between the requested remeasurements and the remeasured events. Missing events were listed and the cycle repeated until a roll had been completely remeasured. The events were then processed by the same geometry and kinematics programs as the PEPR measured events.

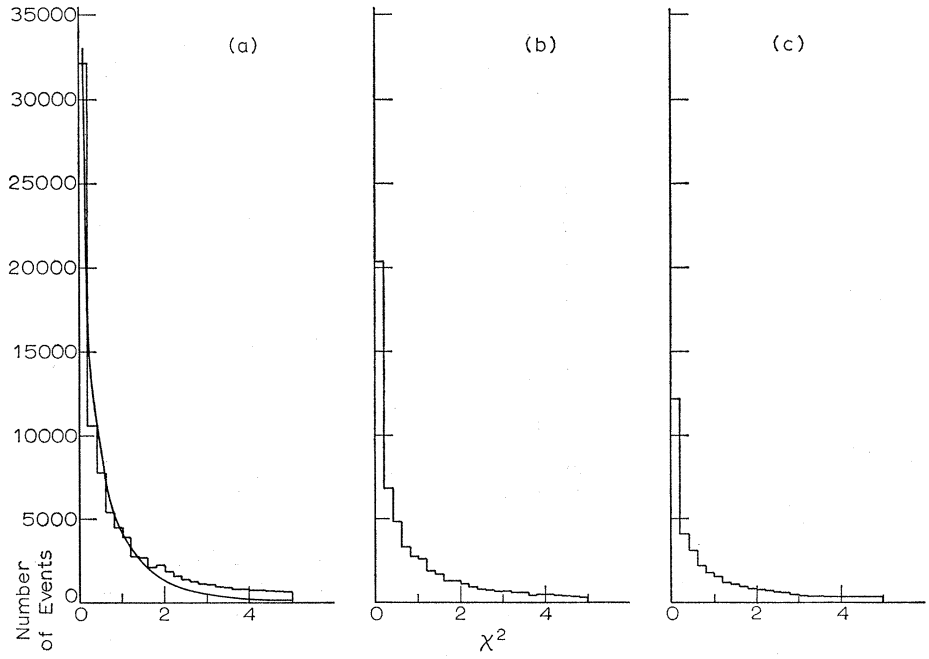

FIG. 22. 1C χ^2 distributions for the fit to $\Sigma^- \rightarrow n+\pi^-$ at decay for (a) the final sample, (b) the PEPR sample, and (c) the hand-measured sample.

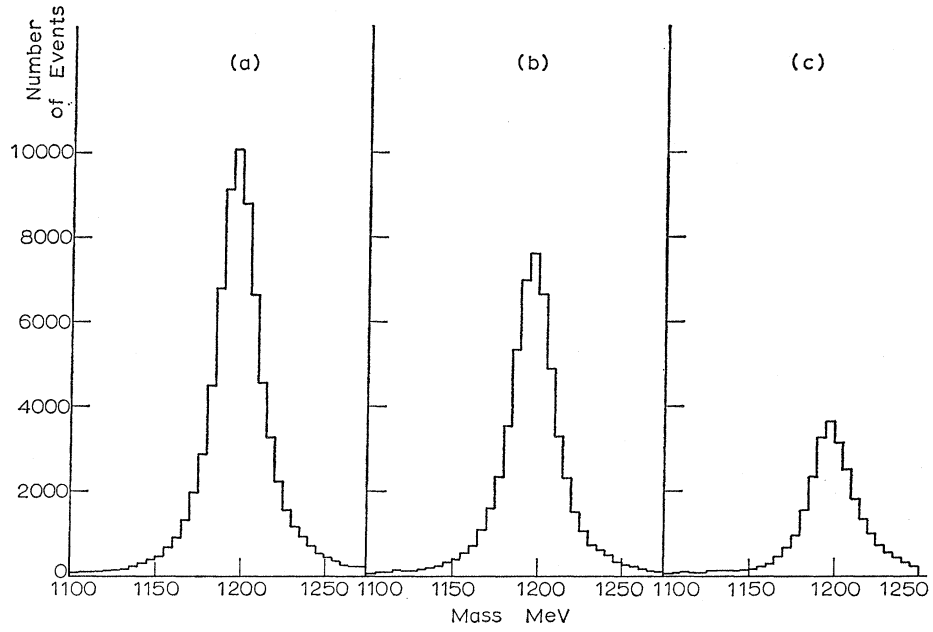

FIG. 23. Mass of the Σ^- calculated from the 3C and 1C fits to Σ^- production for (a) the final sample, (b) the PEPR sample, and (c) the hand-measured sample.

VII. PIONIC DECAY ASYMMETRY

A. Monte Carlo Generation of Leptonic and Pionic Decay Samples

An attempt was made to evaluate possible background asymmetries with the aid of a set of Monte-Carlo-generated decay samples. A "sublibrary" tape, containing only events with constrained Σ production and good decay fits, was generated from the 17 packed library tapes. Only the following quantities were preserved on this sublibrary: (a) event number; (b) x, y, z of the production vertex; (c) momentum of the K^- at production; (d) momentum of the π^+ at production; (e) momentum of the Σ at decay; (f) momentum of the decay product at decay, interpreted as a π; (g) length of the Σ.

These data were sufficient to use as starting values for various Monte Carlo calculations. The first question studied may be formulated as follows: Given the experimental sample of Σ^- measured and fitted at production, is this sample such that if one allows the Σ to decay isotropically in the Σ center of mass (and examines

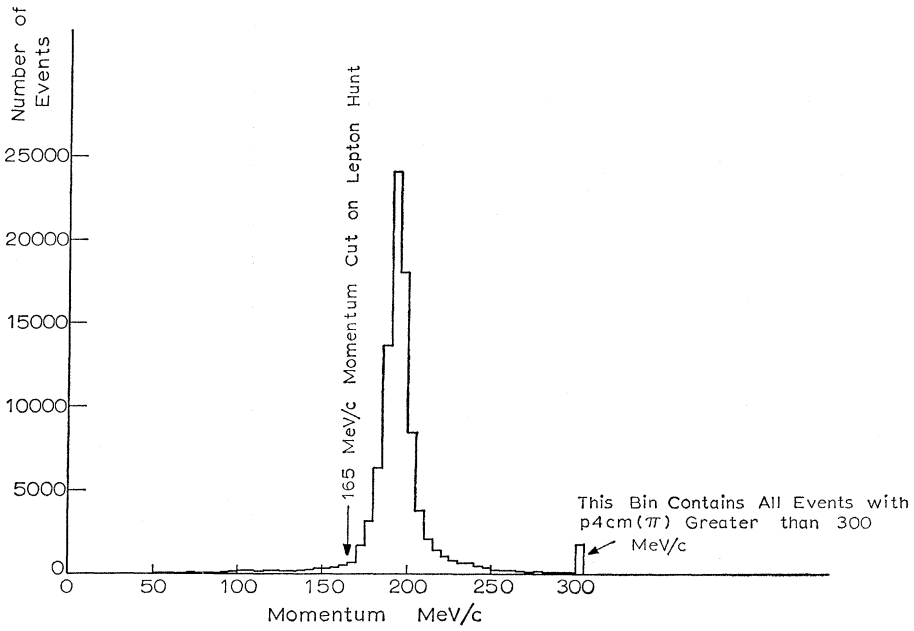

FIG. 24. Measured momentum of the decay track, interpreted as a π, plotted in the Σ^- center-of-mass system.

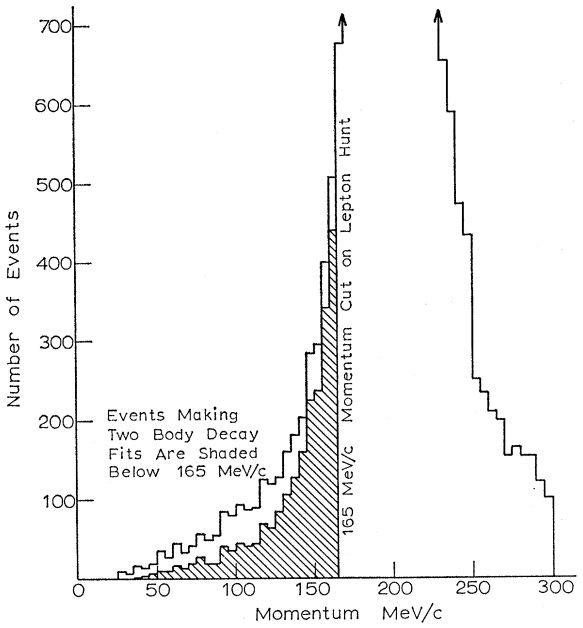

FIG. 25. Measured momentum of the decay track, interpreted as a π, plotted in the Σ^- center-of-mass system, with the scale of Fig. 24 expanded by a factor of 50 to display the tail of the spectrum.

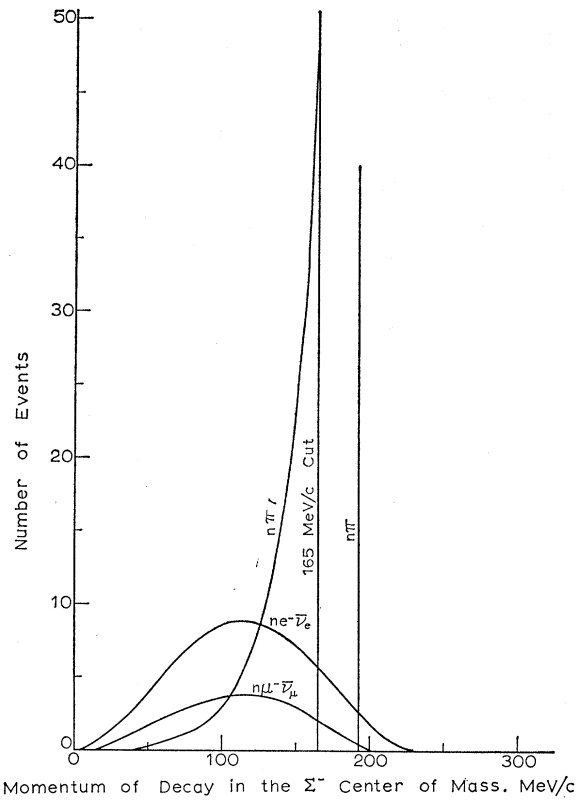

FIG. 26. Relative phase space for the e^- and μ^- decays of the Σ^- hyperon together with the normalized radiative π^- decay spectrum. The vertical scale is the number of events per 10 MeV/c.

such decays with the same cutoffs and algorithms used in the course of the experiment), will the resultant decay spectrum still be found to be isotropic, or will it now contain an asymmetry?

The Monte Carlo program proceeded as follows. The momentum of the Σ at production, as calculated from the K^- and π^+, and the position of the production vertex were used as starting values. A Σ length was drawn at random from an exponential distribution. If the residual range corresponding to this length was negative, the Monte Carlo Σ was assumed absorbed and no decay was generated. If positive, the range was converted to a momentum for the Σ at decay. The position of the decay vertex was calculated. An isotropic decay direction was now specified in the Σ rest frame and a momentum was selected (a) according to the appropriate Fermi phase space for leptonic decays or (b) as 192 MeV/c for Monte Carlo pionic decays. The momentum thus selected was then translated to the laboratory system from the Σ rest system at decay, and a laboratory spectrum corresponding to an isotropic center-of-mass decay from the experimental Σ production sample was thereby generated.

A routine to propagate the track in a helical orbit with the appropriate mass interpretation was written. Each decay track was propagated in small bites, continually asking (a) if the range had exceeded the available momentum or (b) if the track had left the chamber or (c) if it had turned through 180°, since that was as far as it would have been measured. One thus obtained the end point and length for a Monte-Carlo-generated decay track. One could then apply the following cuts which correspond to those made on leptonic candidates during lepton hunts. The decay track was ignored if: (1) $|\tan\lambda|>2.0$ (where λ is the dip angle); (2) the production vertex lay outside $2.0<z<28.0$; (3) the length of the longest chord was <10.0 cm.

A momentum cut corresponding to that made on remeasurement candidates was imposed on Monte Carlo leptons. Since the measured decay track was always interpreted as a π, the appropriate correction to convert the e^- or μ^- Monte Carlo spectrum to π^- mass interpretations was performed at this point. The program was run for both e^- and μ^- mass interpretations, the principal differences arising from the different masses in the Fermi phase space and in the helical track propagation.

The output of this Monte Carlo program was a tape in the same format as the sublibrary tape, except that the momenta of the Σ and the decay track, and the length of the Σ, were Monte Carlo generated, and only the events which survived the cuts were present.

B. Likelihood Calculation of α_-

Several measurements of the asymmetry parameter in the decay $\Sigma^-\rightarrow n+\pi^-$ have been reported.[20–22] The

[21] R. Bangerter, thesis, UCRL Report No. UCRL-19244, 1969 (unpublished). Also see R. Bangerter, A. Barbaro-Galtieri, J. Berge, J. Murray, F. Solmitz, M. Stevenson, and R. Tripp [Phys. Rev. Letters 17, 495 (1966)] for references to earlier measurements.

[22] W. Heintzelman, thesis, Yale University, 1968 (unpublished).

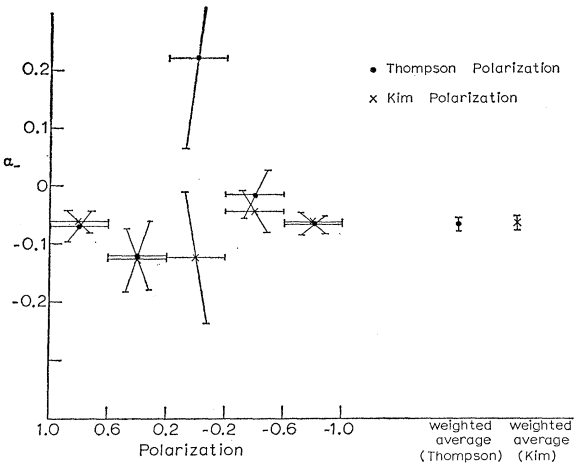

FIG. 27. Independence of α_- and Σ polarization direction. The data were divided into five bins by polarization, and α_- calculated for each set of data. Results from both polarization functions discussed in the text are presented.

evaluation of this parameter from our data was based on the maximum likelihood method. The form of the decay angular distribution given in Eq. (1) leads to a likelihood function

$$L(\alpha_-)=\prod_{i=1}^{N}[1+\alpha_- P_i(\theta_i)\cos\chi_i],$$

where $P_i(\theta_i)$ is the polarization of the Σ^- produced in the reaction $K^-+p\rightarrow\Sigma^-+\pi^+$ evaluated along the direction $\mathbf{p}_{K^-}\times\mathbf{p}_{\pi^+}$ in the center of mass of the production and

$$\cos\chi_i=\frac{\mathbf{P}_i(\theta_i)\cdot\mathbf{p}_n}{|\mathbf{P}_i(\theta_i)||\mathbf{p}_n|},$$

where p_n is the momentum of the neutron in the Σ^- center-of-mass system. The most likely value of α_- is then that value which maximizes $L(\alpha_-)$. For calculational reasons $\ln L(\alpha_-)$ rather than $L(\alpha_-)$ is actually maximized. It can then be shown that in the limit of large statistics, the value of α_- for which $\ln L(\alpha_-)$ is reduced by 0.5 from its maximum value corresponds to 1 standard deviation.

Several sources of bias and background need to be examined. Since no events with projected (on the film) decay angles of less than $\pm 7°$ were accepted during scanning, the effect of this exclusion on α_- must be considered. Heintzelman[22] has shown that as long as events are removed symmetrically with respect to a plane perpendicular to the production normal, the maximum likelihood value of α_- is unaffected. Thus this scanning cut should have no effect as long as the production is azimuthally symmetric with respect to the film plane. To check that this is the case, α_- was calculated as a function of both the laboratory and center-of-mass decay angles, and α_- remains constant, within errors, for this selection. Figure 27 shows that the value of α_- calculated from events selected according to their polarization also remains constant even though the polarization changes sign.

The effect of the rotation of the Σ^- spin direction between production and decay due to the precession of the magnetic moment according to the equation[22]

$$\frac{d\mathbf{s}}{dt}=\boldsymbol{\mu}\times\mathbf{H}$$

was also taken into account in the calculation, using the $SU(3)$ prediction for the Σ^- magnetic moment.[23] This effect on α_- was found to be negligible.

Finally, since the beam was highly asymmetric in this bubble chamber and since cuts on the Σ^- and decay track lengths were employed, a Monte Carlo background calculation was made as described in Sec. VII A assuming that the decay in the center-of-mass system of the Σ^- was isotropic. The result of this calculation yielded a (background) value of $\alpha_-=+0.013\pm 0.015$. Since this background value is consistent with zero, it was subsequently ignored.

It should be pointed out that our value for α_- is uncertain to the extent that the polarization function computed from an amplitude analysis of Σ^- production in K^-p collisions is uncertain. The polarization function used in this experiment was obtained by Thompson[24] and is shown in Fig. 28. This function agrees reasonably well with the polarization function obtained earlier by Tripp *et al.*,[25] but differs, especially for backward Σ^- at $p_{K^-}>400$ MeV/c, with a function computed by Thompson from the analysis of Kim.[2] This latter function is also shown in Fig. 29 and the effect of this difference may be seen in Fig. 27 where the values of α_- obtained from both polarization functions are shown. Since the Thompson polarization function contains more complete data from neutral channels in the $\Lambda(1520)$ region, we have used it rather than the function based on Kim's earlier analysis. This yields the result that $\alpha_-=-0.067\pm 0.011$.

Since the event sample used for this calculation included only those for which both good production and good decay fits were made, the contamination from K^-p elastic scatters is considered to be negligible. That the kinematic overlap between K^-p and $\Sigma^-\pi^+$ final states is small is indicated by the fact that in a careful study of approximately 100 K^-p events with marginal fits, no examples of $\Sigma^-\pi^+$ were found.

VIII. LEPTON IDENTIFICATIONS

A. Lepton Search

The output library of the Yale Kinematic Analysis Program (YACK) was organized so as to maintain both the frame ordering and the experimental structure of

[23] S. Coleman and S. Glashow, Phys. Rev. Letters 6, 423 (1961).
[24] J. Thompson (private communication).
[25] R. Tripp (private communication).

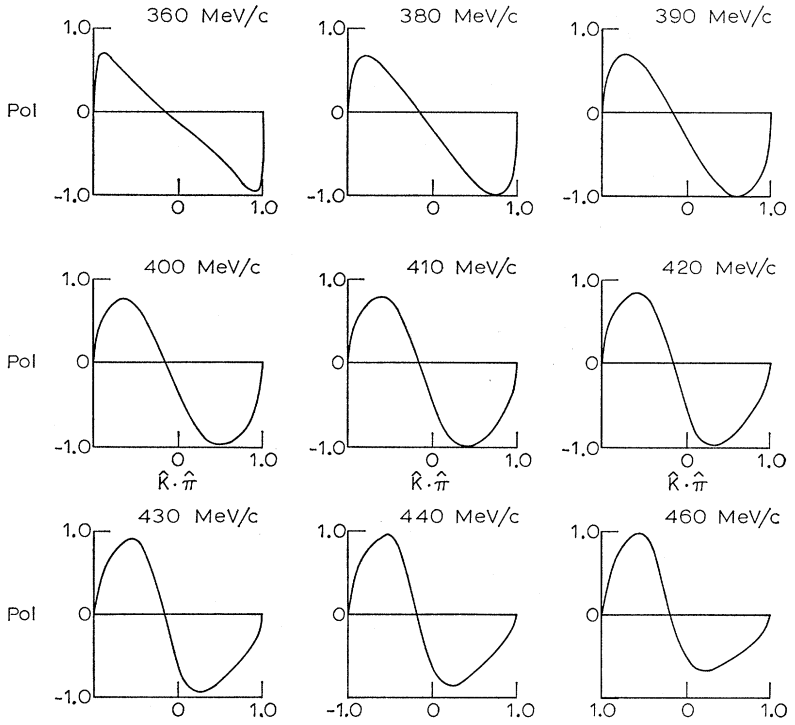

FIG. 28. Σ^- polarization as a function of $\hat{K}\cdot\hat{\pi}$ from the amplitudes of Thompson, at various K^- momenta.

the data. This library was analyzed by a flagging program which applied the following criteria:

(1) Events with no satisfactory production fit or with no reconstructed decay track (unless a K^-p production fit was accepted as discussed in Sec. VI) were flagged "*R*" (remeasure).

(2) Events with satisfactory Σ^- production for which the production vertex had a z coordinate between 2.0

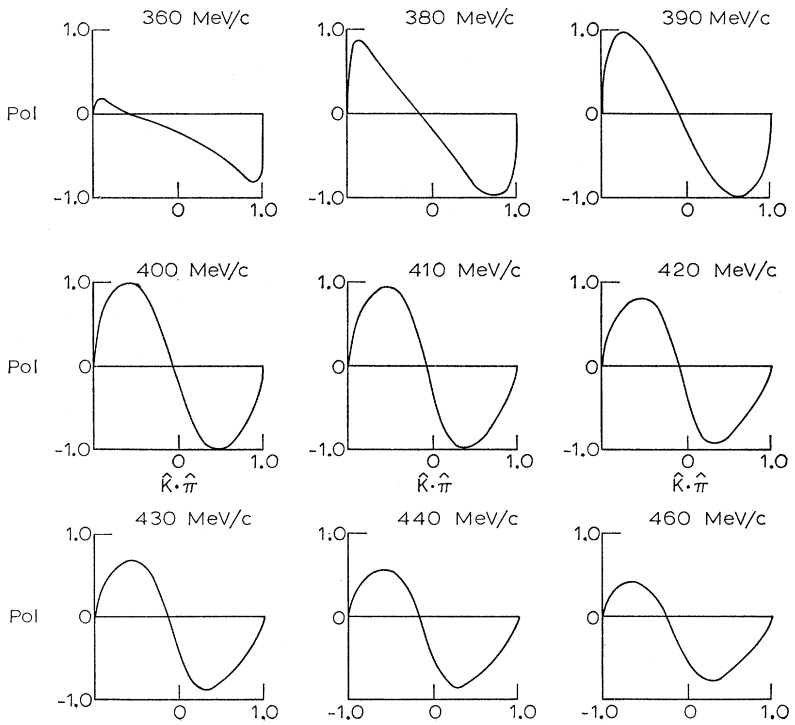

FIG. 29. Σ^- polarization as a function of $\hat{K}\cdot\hat{\pi}$ from the amplitudes of Kim, at various K^- momenta.

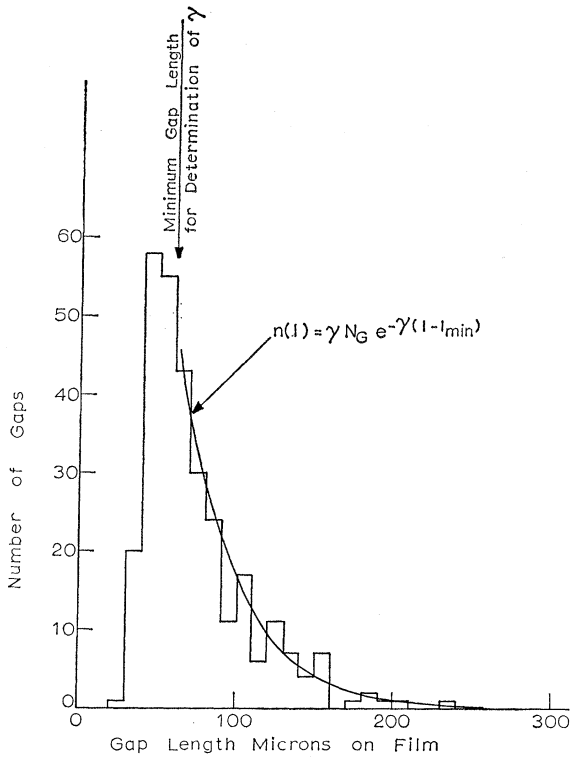

FIG. 30. A typical gap-length distribution consisting of 301 gaps. For a choice of $l_{\min}$ equal to 60 μ, there are 167 gaps of a length greater than $l_{\min}$ and $\gamma=0.0274$.

and 28.0 cm, and for which the decay track has a $|\tan\lambda|<2.0$ and a projected chord in some view greater than 10 cm, were flagged if the *measured* momentum of the decay track in the (fitted) Σ^- center-of-mass system was less than 165 MeV/c. This cut is discussed in Sec. V.

The entire sample of flagged events was then remeasured on the image-plane digitizing machines discussed above and every event not flagged "R" was carefully examined in all views by a physicist, assisted by a complete printed kinematical analysis. First, "non-events" such as K^-p scatters with subsequent K^- decay, $\Lambda\pi\pi$ events, and $\Sigma^-\pi^+\pi^0$ production events were discarded. Secondly, all decay tracks in the sample were carefully examined for kinks, disappearances or abrupt changes in ionization. Estimates of ionization, optimum views for gap measurement, and features of the event to be examined under high magnification were recorded. Of the entire sample of approximately 4500 second remeasurements performed, about 20% were examined by a physicist. The great majority of these events were found not to be leptonic events but rather non-events, kinks, short decay tracks, Σ^- absorption events, or obvious radiative decays.

The sample of second remeasurements, except for non-events, was then processed through geometry, kinematics, library, and flagging routines. All events which were flagged during either of the two final passes and which were not ruled out as leptonic candidates by previous inspection and which consistently failed to exhibit a decay track momentum (in the $\Sigma^-_{\text{c.m.}}$) greater than 165 MeV/c were subjected to a final examination under high magnification. Those events which appeared to be well measured and had a decay track conceivably near minimum ionization were then selected for gap measurement.

B. Gap-Length Distributions

In order to select leptonic events out of the sample still remaining after at least two remeasurements and visual inspection, each candidate was subjected to a gap-length distribution analysis. This procedure provided an objective criterion for selection although the statistical uncertainties were large in many cases.

The probability $P(l)$ of forming a bubble in the length dl, after traveling a distance l since the previous bubble, obeys the equation[26]

$$\frac{dP(l)}{dl}=-\gamma P(l), \tag{5}$$

where $\gamma=F/\beta^2$, β being the velocity of the particle and F being a function of the track and chamber geometry and of the chamber operating conditions. Thus if we define a gap as the distance between bubble centers, the number of gaps with lengths between l and $l+dl$ is given by

$$n(l)dl=N(l_{\min})e^{-\gamma(l-l_{\min})}dl, \tag{6}$$

where $l_{\min}$ is the minimum gap length observable and $N(l_{\min})$ is the total number of gaps of length $l>l_{\min}$. This distribution has the property that once the value of $l_{\min}$ which best fits the data has been determined, the value of γ is given by

$$1/\gamma=\bar{l}_{l>l_{\min}}-l_{\min}, \tag{7}$$

where $\bar{l}_{l>l_{\min}}$ is simply the average gap length for gaps of length greater than $l_{\min}$. The bubble diameter does not affect this result, except as it determines $l_{\min}$, and in fact does not even appear since gaps are measured between bubble centers.

In order to eliminate the unknown function F and thus to determine β^2, it was necessary to measure a calibration track, and this was always chosen to be either the π^+ or the K^- involved in the event in order to be sure that the operating conditions were identical with those for the lepton candidate. The kinematic analysis program computed, in each view, an expected

[26] R. L. Gluckstern, Nucl. Instr. Methods 45, 166 (1966).

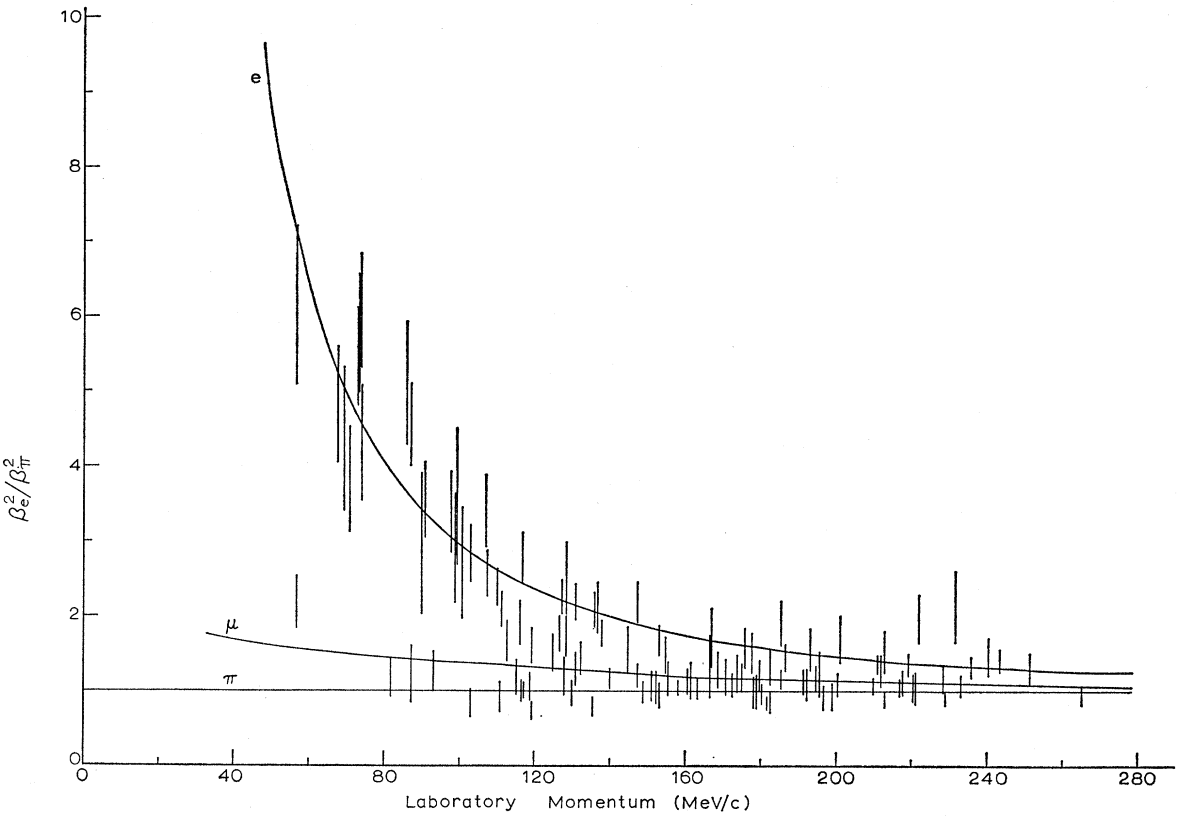

FIG. 31. Plot of β_e^2/β_π^2 against the laboratory momentum of the decay track.

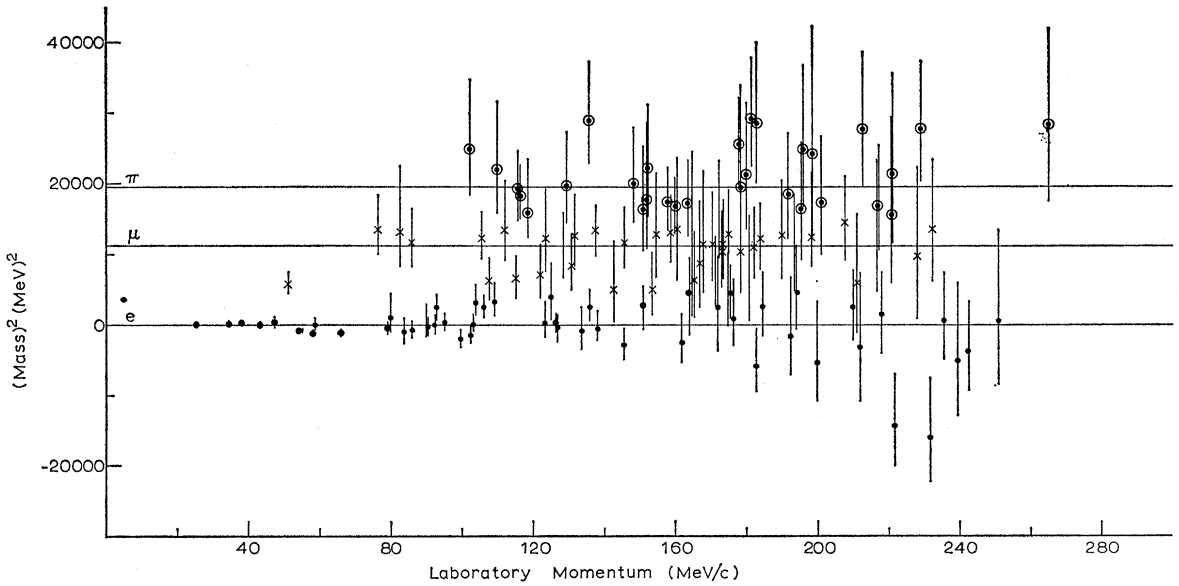

FIG. 32. Plot of (mass)² against the laboratory momentum of the decay track. The mass interpretation is based upon the ionization measurements as discussed in the text.

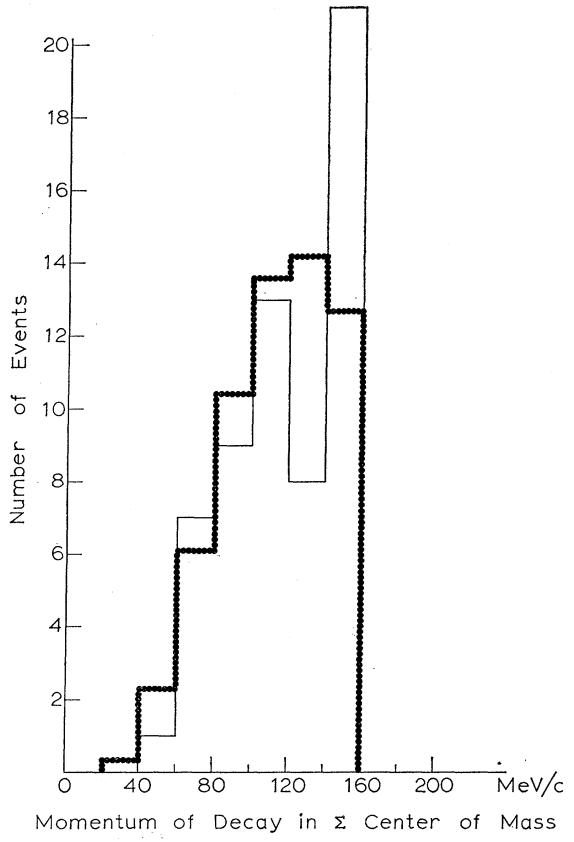

FIG. 33. Experimental and Monte Carlo spectra for 60 e^- events. The solid line represents the experimental data, and the dots represent Monte Carlo phase space for 60 e^- with a momentum in the Σ^- center-of-mass system less than 160 MeV/c. Note the contamination from unresolved radiative π decays in the 140–160-MeV/c bin.

ionization for each track on the film given by

$$I=G/\beta^2, \tag{8}$$

where G is a function of chamber and track geometry approximately independent of mass interpretation, and the velocity β was computed assuming the masses involved in normal Σ^- production and (two-body) decay. It is important to note that $F=GC$, where C is a function of chamber operating conditions only and is thus the same for all tracks in the event. Thus

$$\frac{\gamma_c}{\gamma_l}\frac{I_{\pi^-}}{I_c}=\frac{\beta_l^2}{\beta_{\pi^-}{}^2}, \tag{9}$$

where $1/\gamma_c$ and $1/\gamma_l$ are the measured average gap lengths for the calibration track and the lepton candidate, while I_c and I_{π^-} are the computed ionizations for the calibration track and for the lepton candidate treated as a π^-. The resulting ratio, which in principle identifies the decay particle, has a fractional error given by

$$\pm\left(\frac{1}{N_c}+\frac{1}{N_l}\right)^{1/2},$$

where N_c and N_l are the number of gaps measured on the calibration and lepton candidate tracks, respectively.

The gap-length measurements were performed on a digitized microscope with an over-all magnification of 60. Gaps were recorded between bubble centers. The centers of curvature of beginnings or ends of "blobs" also defined ends or beginnings of gaps. Measurements were recorded on paper tape which was then read by the PDP-6 computer. The gap lengths were then histogrammed and a series of curves representing the function $n(l)$ given in Eq. (6) for values of $l_{\min}$ from 0 to 100 μ were plotted on the computer display scope. The operator could then select the curve which best fit the data for each event. Typically this corresponded to a value for $l_{\min}$ of 50 μ. An example of a gap-length distribution and the fitted curve for a particular $l_{\min}$ is shown in Fig. 30.

The results of these measurements on a sample of events selected by physicists as possible leptonic decays are shown in Fig. 31. At lower laboratory momentum the resoltuion is satisfactory. Because of the confusion at higher momenta, a program was written to compute the mass of each candidate based on the expression

$$M^2=(\beta_\pi{}^2/\beta_l{}^2)(P_l{}^2/P_\pi{}^2)(M_\pi{}^2+P_\pi{}^2)-P_l{}^2,$$

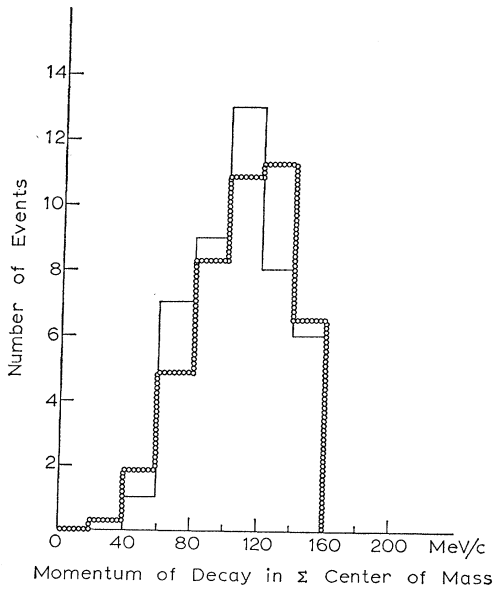

FIG. 34. Experimental and Monte Carlo spectra for 44 e^- events. The solid line represents the experimental data, with the cut that only events with a laboratory momentum less than 160 MeV/c have been kept in the region where the decay track has a momentum in the range 140–160 MeV/c in the Σ^- center-of-mass system. The dots represent the Monte Carlo phase space for 44 e^-, with the same cuts as the experimental data.

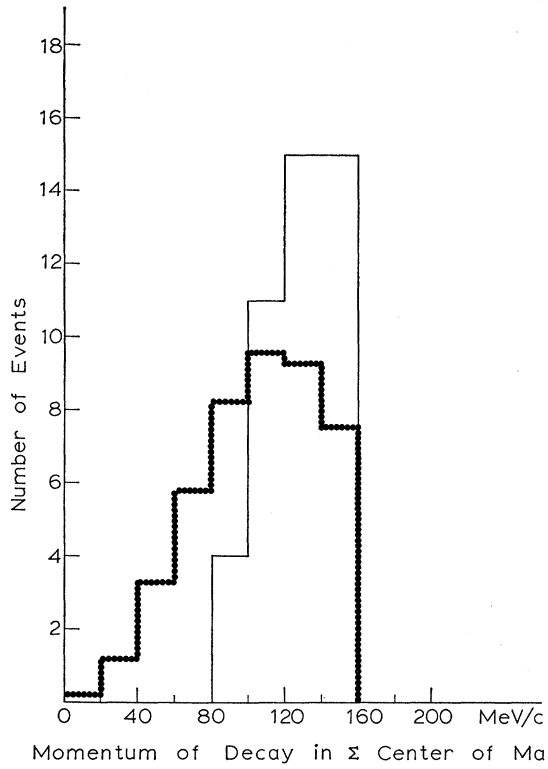

FIG. 35. Experimental and Monte Carlo spectra for 45 μ^- events. The solid line represents the experimental data, and the dots represent the Monte Carlo phase space for 45 μ^- with a momentum in the Σ^- center-of-mass system less than 160 MeV/c. Note the overabundance of events from unresolved radiative π decays.

where the subscript π refers to the π^- interpretation and the subscript l refers to the lepton interpretation. Three mass values were computed for each candidate using the values of P_l appropriate to pion, muon, and electron interpretations. The mass value closest to one of these three known masses (in terms of the now asymmetric error) was then used to assign a final interpretation to the candidate. The measured masses for the assigned interpretations are shown in Fig. 32.

C. Spectra and Cuts

The gap-measurement procedure and the resulting mass determinations described above produced 60 events with an e^- assignment, 48 events with a μ^- assignment, and 29 events with a π^- assignment. Because of the statistical inaccuracies in gap measurement, however, the events with e^- and μ^- assignments were highly contaminated by the radiative decay $\Sigma^- \rightarrow n\pi^-\gamma$ at momenta above 140 MeV/c for the decay track (interpreted as a π^-) in the Σ^- center-of-mass system.

As discussed in connection with Fig. 26, the *a priori* probability that the decay is radiative rather than leptonic becomes overwhelming at high momenta. This effect is evident in Fig. 33, where we plot the spectrum of the 60 e^- events (interpreted as π^- in the c.m. transformation so that the 160-MeV/c cut has meaning) together with the expected phase-space spectrum as generated by the Monte Carlo routines described in Sec. VII. The obvious excess of events above 140 MeV/c was eliminated by using only those events in this bin for which the laboratory momentum was less than 160 MeV/c and for which reliable gap measurements could thus be made. The results of this cut together with the modified Monte Carlo spectrum are shown in Fig. 34. Because of the poorer mass resolution for μ^- decays, only those μ^- were used which had a laboratory momentum of less than 150 MeV/c. The equivalent spectrum for the μ^- events is shown in Figs. 35 and 36 along with the Monte Carlo phase space. These cuts reduced the sample to 44 e^- events and 19 μ^- events.

Events in which the π^- from normal, two-body decay of the Σ^- itself decays into a μ^- in a short distance and at an undetectable angle constitute an unremovable background to the sample of μ^- events. This background was estimated to be 6 ± 4 events from the results of a Monte Carlo program employing the same rejection criteria as were employed in this experiment.

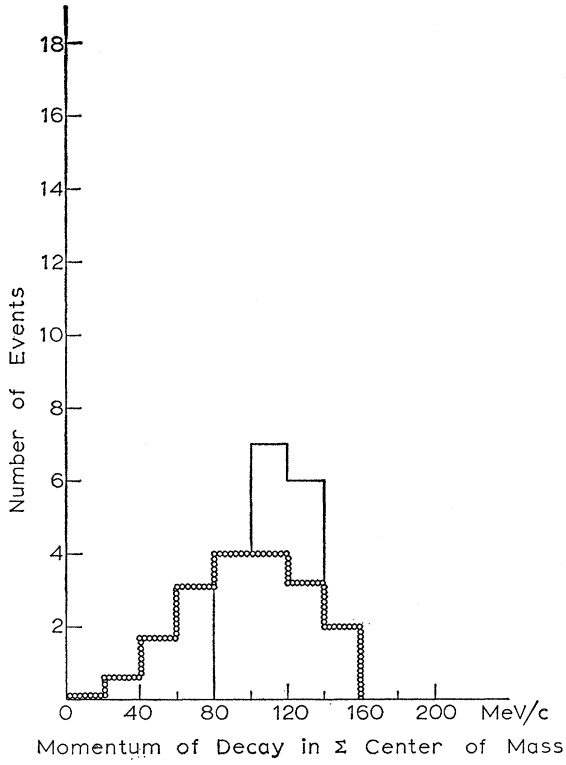

FIG. 36. Experimental and Monte Carlo spectra for 19 μ^- events. The solid line represents the experimental data, and the dots the Monte Carlo phase space for 19 μ^- with the cut that the laboratory momentum must be less than 150 MeV/c for all momenta in the Σ^- center-of-mass system applied. This cut is more restrictive than that applied to the e^- spectrum owing to the increased difficulty of resolving μ^- from radiative π decays.

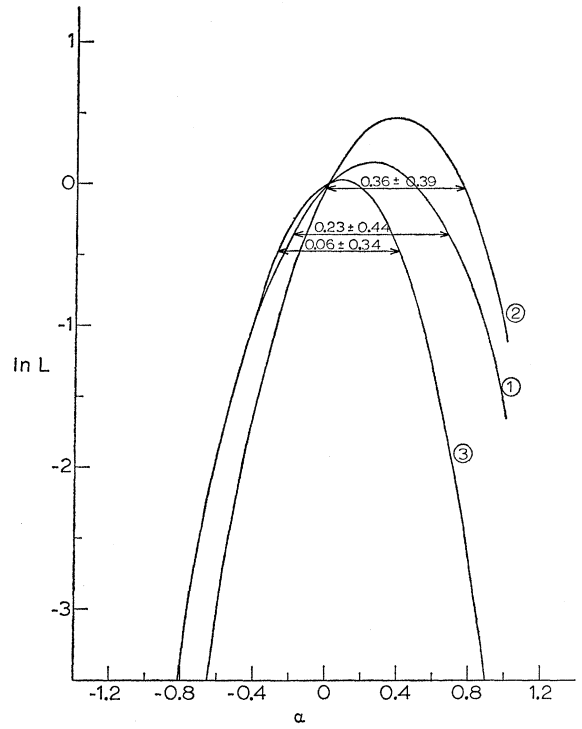

FIG. 37. Likelihood functions for α_{lept} using the polarization function of Thompson for (1) the 44 e^- events, (2) the 44 e^- and 19 μ^- events, and (3) background events.

IX. LEPTONIC DECAY ASYMMETRY

In order to facilitate selection and sorting, all of the 137 events which had been subjected to gap measurement were recorded on punched cards and this deck was then subjected to analysis by a program very similar to that used for the evaluation of the two-body decay asymmetry discussed in Sec. VII. This program made a number of checks to ensure that no events were used where either the projected length of the Σ^- was less than 1 mm in all views or where the momentum of the Σ^- at the decay point was less than 70 MeV/c. This cut was necessary in order to eliminate events in which the Σ^- was absorbed at rest rather than decaying in flight. As in Sec. VII, a likelihood function was calculated which now, however, displays the lepton velocity (the negative of the helicity) explicitly, i.e.,

$$L(\alpha)=\prod_{i=1}^{N}[1+\alpha\beta_i P_i(\theta_i)\cos\chi_i],$$

where $\cos\chi_i$ is in this case given by

$$\cos\chi_i=\frac{\mathbf{P}_i(\theta_i)\cdot\mathbf{p}_l}{|\mathbf{P}_i(\theta_i)|\,|\mathbf{p}_l|},$$

where P_l is the momentum of the lepton in the Σ^- center-of-mass system and β_i is the lepton velocity. The value of α which maximizes $\ln L(\alpha)$ is computed as before.

Owing to statistical considerations, the shape and the location of the maximum in the likelihood functions for the asymmetry in the leptonic events depends much more sensitively on the polarization function used than did the likelihood functions for the two-body decay asymmetry. In Figs. 37 and 38 we show the likelihood functions, computed using the two polarization functions discussed in Sec. VII, for the selected lepton events, for the selected electron events only, and for the events not selected.

Using Thompson's most recent polarization function,[24] we find

$$\alpha_{\text{lept}}(e^- \text{ events only})=+0.23\pm0.44,$$
$$\alpha_{\text{lept}}(e^- \text{ and } \mu^- \text{ events})=+0.36\pm0.39.$$

We have also computed α_{lept} for our events using the polarization function which was used by Gershwin *et al.*[4] The agreement with the above values is good both in the values and in the errors.

X. CONCLUSION

We have used the relationship given in Eq. (3) to obtain a value of g_A/g_V from our data. While this ex-

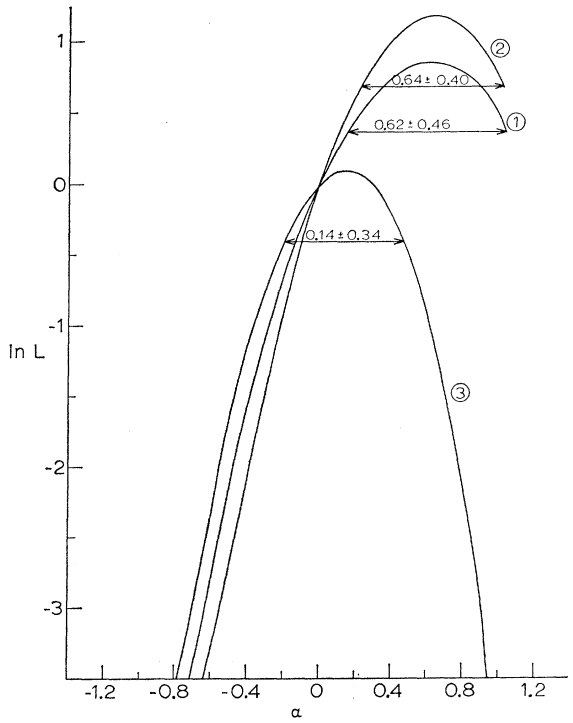

FIG. 38. Likelihood functions for α_{lept} using the polarization function of Kim for (1) the 44 e^- events, (2) the 44 e^- and 19 μ^- events, and (3) background events.

pression is only approximate, the corrections are expected to be quite small[4] and completely negligible given the statistical uncertainty in our value of α_{lept}. Using both the electron and muon events, our result is

$$g_A/g_V = -0.33_{-0.85}^{+0.30}.$$

This result favors a negative sign for g_A/g_V, in disagreement with the Cabibbo theory, but cannot exclude a positive sign. Since the measurement of α_{lept} by Gershwin[27] for a similar sample of polarized Σ^- yields a value for g_A/g_V of $+0.19_{-0.17}^{+0.20}$, in agreement with the Cabibbo theory, a substantial increase in the number of events will be required to make a definitive determination of the sign.

ACKNOWLEDGMENTS

We are indebted to Professor Joseph Lach for assistance with the Monte Carlo programs, to Dr. Julia Thompson for providing polarization data, and to Dr. N. S. Wong, Dr. T. Ludlam, and Dr. W. Heintzelman for assistance with the wire measuring system and for many useful discussions. The successful operation of the Yale PEPR system was based on many years of development by the MIT group under Professor I. Pless as well as on the effective work of the Yale technical staff involving particularly Walter Lund, Peter Martin, Osborne Murphy, Blaize Lombardi, and Monroe Fisch. Dr. T. Ferbel assisted in the early stages of this development. The patient and devoted work of the scanning and measuring staffs at Yale, Brookhaven, and the University of Massachusetts is also gratefully acknowledged. Dr. S. Herzback and Dr. J. Schaffer of the University of Massachusetts also contributed to the early stages of this experiment. Dr. Orin Hansen and Mrs. Rochelle Lauer contributed greatly to the programming system, and the cooperation and assistance of the Yale Computer Center staff and the NYU Computer Center staff were invaluable. Finally, we wish to thank the National Science Foundation for their support during the period of this research and the U. S. Atomic Energy Commission for their patient and generous support of the development of the Yale PEPR system.

[27] L. Gershwin, thesis, UCRL Report No. UCRL-19246, 1969 (unpublished).